FORWARD GENETICS IN *C. ELEGANS* REVEALS GENETIC ADAPTATIONS TO POLYUNSATURATED FATTY ACID DEFICIENCY

Delaney Kaper[1], Uroš Radović[1], Per-Olof Bergh[2], August Qvist[1], Marcus Henricsson[2], Jan Borén[2] and Marc Pilon[1]

Affiliations: [1]Department of Chemistry and Molecular Biology, University of Gothenburg, Gothenburg, Sweden, [2]Department of Molecular and Clinical Medicine/Wallenberg Laboratory, Institute of Medicine, University of Gothenburg, Gothenburg, Sweden.

Running Title:

A *fat-2* Suppressor Screen

Corresponding author:

Marc Pilon

Email: marc.pilon@cmb.gu.se

ABSTRACT

Polyunsaturated fatty acids (PUFAs) are essential for mammalian health and function as membrane fluidizers and precursors for signaling lipids though the primary essential function of PUFAs within organisms has not been established. Unlike mammals who cannot endogenously synthesize PUFAs, *C. elegans* can *de novo* synthesize PUFAs starting with the Δ12 desaturase FAT-2 which introduces a second double bond to monounsaturated fatty acids to generate the PUFA linoleic acid. FAT-2 desaturation is essential for *C. elegans* survival since *fat-2* null mutants are non-viable; the near-null *fat-2(wa17)* allele synthesizes only small amounts of PUFAs and produces extremely sick worms. Using fluorescence recovery after photobleaching (FRAP), we found that the *fat-2(wa17)* mutant has rigid membranes and can be efficiently rescued by dietarily providing various PUFAs, but not by fluidizing treatments or mutations. With the aim of identifying mechanisms that compensate for PUFA-deficiency, we performed a forward genetics screen to isolate novel *fat-2(wa17)* suppressors and identified four internal mutations within *fat-2*, and six mutations within the HIF-1 pathway. The suppressors increase PUFA levels in *fat-2(wa17)* mutant worms and additionally suppress the activation of the *daf-16*, UPR^{er} and UPR^{mt} stress response pathways that are active in *fat-2(wa17)* worms. We hypothesize that the six HIF-1 pathway mutations, found in *egl-9*, *ftn-2*, and *hif-1* all converge on raising Fe^{2+} levels and in this way boost desaturase activity, including that of the *fat-2(wa17)* allele. We conclude that PUFAs cannot be genetically replaced and that the only genetic mechanism that can alleviate PUFA-deficiency do so by increasing PUFA levels.

INTRODUCTION

The fluidity of cellular membranes is heavily influenced by the saturation level of the phospholipids composing the membrane. Phospholipids containing saturated fatty acid (SFA) tails are more tightly packed and therefore form more rigid membranes, while phospholipids with an abundance of unsaturated fatty acids (UFAs) are more loosely packed and result in fluid membranes [1,2]. Polyunsaturated fatty acids (PUFAs) themselves can also affect many different cellular processes and are precursors to both anti- and pro-inflammatory PUFA-derived signaling molecules called eicosanoids [3–6]. Imbalances between SFAs and PUFAs are associated with chronic diseases including coronary heart disease, diabetes, hypertension, and renal disease [4].

C. elegans PAQR-2, and its mammalian ortholog AdipoR2, promote the production and incorporation of PUFAs into phospholipids to restore membrane homeostasis [7]. Whether this is the primary function of PUFAs in cells or organismal physiology is still not resolved. In particular, no unbiased forward genetic screens for suppressors of PUFA deficiency have been reported. Mammals are not able to endogenously synthesize PUFAs and must obtain omega-3 and omega-6 PUFAs from the diet, a fact known since 1930 [8,9]: linoleic acid (LA, 18:2n6) and alpha-linolenic acid (ALA, 18:3n3) must be dietarily supplied and can be further desaturated and elongated into ≥20-carbon PUFAs used structurally or as precursors of signaling molecules [10]. An exception to this exists during severe essential fatty acid deficiency when mammals can synthesize mead acid (20:3n9), though this is not a common occurrence [11]. In contrast, *C. elegans* expresses many desaturases and elongases that can convert dietary or de novo synthesized SFAs into a wide range of PUFAs: Δ9 desaturases are responsible for converting SFAs into monounsaturated fatty acids (MUFAs) by adding a first double bond, a Δ12 desaturase adds an additional double bond to transform MUFAs into LA, a PUFA with two double bonds, and Δ5 and Δ6 desaturases introduce additional double bonds to produced PUFAs with three, four or five double bonds [12–14]. To better understand the essential roles of PUFAs in cells and whole organisms, we leveraged a mutant allele of the *C. elegans* Δ12 desaturase FAT-2, whose function is to convert oleic acid (OA, 18:1n9) into linoleic acid (LA, 18:2n6) [15] (**Fig 1A**). Because this is a critical step for PUFA production, worms devoid of FAT-2 activity (i.e. *fat-2(-)* null mutants) are not able to synthesize any PUFAs and are not viable. In contrast, the *fat-2(wa17)* allele produces a partially functional protein bearing a S101F substitution (**Fig 1B-C**): mutants homozygous for this allele produce <10% of the normal levels of PUFAs and are extremely slow growing and sickly but, crucially, are viable [10].

Although there is no mammalian homolog of FAT-2 [16], the *fat-2(wa17)* mutant can still serve as a useful genetic model to reveal evolutionarily conserved roles of PUFAs in organisms, and to help identify mechanisms that can compensate for PUFA deficiency. Here, we began by characterizing the *fat-2(wa17)* mutant in terms of its ability to be rescued with dietary PUFAs or with mutations previously

identified as suppressors of *paqr-2(tm3410)* mutant phenotypes that are attributed to membrane rigidity. We then performed an exhaustive forward genetic screen for *fat-2(wa17)* suppressors in the hope that the critical functions of PUFAs could be discovered and to identify mechanisms that allows cells/organisms to cope with PUFA deficiencies. This screen yielded ten *fat-2(wa17)* suppressor alleles that fell into two groups: mutations within *fat-2* itself, and mutations in the *hif-1* pathway that converge on inhibition of *ftn-2* expression.

RESULTS

Characterization of the *fat-2(wa17)* mutant

The severe growth defect of *fat-2(wa17*) mutants can be suppressed by the wild-type *fat-2(+)* allele carried on an extrachromosomal array, confirming that this growth defect is due to reduced *fat-2* activity (**Fig 2A**). As expected, given their low amounts of PUFAs, fluorescence recovery after photobleaching (FRAP) shows that the membranes of intestinal cells in the *fat-2(wa17)* mutant are excessively rigid and indeed appeared as rigid as those of the *paqr-2(tm3410)* mutant characterized by an excess of SFAs in its phospholipids [17,18] (**Fig 2B-C**).

Also as expected, low doses of dietary linoleic acid (LA, 18:2n6) fully rescued the *fat-2(wa17)* growth defect (**Fig 2D**). This rescue by LA is transient and does not last when the following generation is transferred back to NGM plates (**Fig 2E**), which is consistent with the rapid turnover of fatty acids in *C. elegans* [19]. Eicosapentaenoic acid (EPA, 20:5n3) is the longest and most unsaturated PUFA produced in *C. elegans* (**Fig 1A**) and is also able to rescue the *fat-2(wa17)* mutant, albeit requiring higher concentrations than LA (**Fig 2F**). Surprisingly, docosahexaenoic acid (DHA, 22:6n3), which is not produced by *C. elegans*, is also able to rescue the *fat-2(wa17)* mutant (**Fig 2G**). Temperature has a direct effect on membrane fluidity: given a constant phospholipid composition, lower temperatures cause rigidification while higher temperatures promote fluidity [20]. We found that the *fat-2(wa17)* mutant is growth-arrested when cultivated at membrane-rigidifying 15°C, and conversely shows improved growth at 25°C, which again is similar to earlier findings with the *paqr-2(tm3410)* mutant [21] (**Fig 2H**). However, cultivating the *fat-2(wa17)* mutant in the presence of the non-ionic detergent NP-40, which improves the growth of the *paqr-2(tm3410)* mutant [17], did not suppress the poor growth phenotype of the *fat-2(wa17)* mutant even though it did improve membrane fluidity as measured using FRAP (**Fig. 2I-J**). Similarly, supplementing the *fat-2(wa17)* mutant with the MUFA oleic acid (OA, 18:1), which also suppresses *paqr-2(tm3410)* phenotypes [17], did not suppress the poor growth phenotype of the *fat-2(wa17)* mutant (**Fig 2K**). Conversely, membrane-rigidifying glucose (which causes a high SFA/UFA ratio in the dietary *E. coli* [22]) or the SFA palmitic acid (PA, 16:0) did not exacerbate the growth defect of *fat-2(wa17)* (**Fig 2L-M**). The observations that NP-40 and OA do not rescue *fat-2(wa17)*, and that membrane rigidifying conditions (dietary glucose or PA) were not

detrimental to *fat-2(wa17),* suggest that membrane rigidification may not be the main cause of the *fat-2(wa17)* growth defects.

Lipidomic analysis of phosphatidylcholines (PCs) and phosphatidylethanolamines (PEs) in the *fat-2(wa17)* mutant confirmed its reduced levels of PUFAs relative to wild-type worms (**Fig 3A; S1A Fig)**, with the largest loss observed in longer PUFAs, namely dihomo-γ-linolenic acid (DGLA; C20:3), arachidonic acid or eicosatetraenoic acid (AA or ETA, C20:4) and, most strikingly, EPA (C20:5) (**Fig 3B-C; S1B-C Fig**). Consistent with previous publications [10], the levels of 18:1 fatty acids were greatly increased in the *fat-2(wa17)* mutant. Even though the lipid analysis methods used here are not able to distinguish between different 18:1 species, a previous study showed that the majority of the 18:1 fatty acids in the *fat-2(wa17)* mutant is actually 18:1n9 (OA) [10] and not 18:1n7 (vaccenic acid) as in most other strains [10,23]; this is because OA is the substrate of FAT-2 and thus accumulates in the mutant. As expected, exogenous addition of LA to these worms resulted in an increase of PUFAs, and in particular resulted in elevating EPA levels to more than 12% compared to less than 2% of total fatty acids in the PCs of *fat-2(wa17)*. Transferring *fat-2(wa17)* from LA to NGM 6 hours prior to harvesting did not lessen this increase, suggesting minimal LA depletion during this time (**Fig 3A-C; S1A-C Fig**). Cultivation at 25°C did not result in any significant changes in the *fat-2(wa17)* mutant, indicating that the growth rescue seen at 25°C is not due to increased PUFA levels in the lipidome (**Fig 3A-C; S1A-C Fig**).

Testing the effect of *paqr-2(tm3410)* suppressors

The previously characterized *paqr-2(tm3410)* null mutant has excess SFAs within phospholipids and many of the resulting defects, including membrane rigidity, can be suppressed by mutations that activate fatty acid desaturases or promote the incorporation of UFAs into phospholipids [17,24–26]. Given the phenotypic similarities between *paqr-2(tm3410)* and *fat-2(wa17)*, such as cold intolerance and rigid membranes, we hypothesized that previously characterized *paqr-2(tm3410)* suppressors may be able to suppress *fat-2(wa17)* as well. However, the *paqr-2(tm3410)* suppressors tested (*mdt-15(et14), nhr-49(et8), fld-1(et46), paqr-1(et52), acs-13(et54)*; [17,24–26]) resulted in either no or only slight rescue of *fat-2(wa17)* growth (**Fig 4A-D**). Additionally, Oil Red O staining of *fat-2(wa17)* mutants suggests that they have an excessive lipid content, and this too was not normalized by the tested *paqr-2(tm3410)* suppressors (**Fig 4E-G**). These results suggest that membrane rigidity is at most only a minor cause of the *fat-2(wa17)* defects since fluidizing treatments (NP-40 or OA) or mutations (the tested *paqr-2* suppressors) provide only minimal or no suppression.

A forward genetics screen for *fat-2(wa17)* suppressors

With the aim of identifying essential roles of PUFAs and molecular mechanisms that can compensate for PUFA deficiency, we performed a forward-genetic screen for *fat-2(wa17)* suppressors that allow growth to adulthood within 72 hours, as opposed to the ~120 hours needed for the parental strain (**Fig 5A**). Approximately 40,000 EMS-mutagenized haploid genomes were screened leading to the isolation of ten *fat-2(wa17)* suppressors which fell into two groups: mutations within the *fat-2* locus itself and mutations within genes of the HIF-1 pathway (**Fig 5B-C**). The *fat-2(wa17)* suppressors all reached adulthood within 72 hours (criteria for the screen) and improved the growth of the mutant when assessed by measuring worm length at 72 hours (**Fig 5D-E**). The *hif-1(et69)* mutation was recreated by CRISPR-Cas9 within the *fat-2(wa17)* background to confirm its *fat-2(wa17)* suppressor activity (**S2A Fig**); multiple independent isolations of essentially the same alelles within *egl-9* (alelles *et60-et62)*, *fat-2 (*alleles *et63-et66), and ftn-2(et67-68)* also serves as confirmation for these loci.

Three of the four *fat-2* intragenic alleles (*et64-et66*) carried a substitution of serine to leucine at position 99 (S99L), only two amino acids away from the S101F mutation in *fat-2(wa17)*; the fourth, *et63*, is a missense mutation substituting valine with methionine at position 25 (V25M) **(Fig 5B).** These four internal *fat-2* alleles likely compensate structurally for the S101F mutation in *fat-2(wa17)* and thus improve its activity.

Three independent *fat-2(wa17)* suppressor mutations were found to affect the same arginine at position 557 of EGL-9 (*et60 and et61* resulted in a R557H missense while *et62* caused a R557C missense; **Fig 5B**). EGL-9 is a proline hydroxylase (PHD) that interacts via its R557 with Fe^{2+}/2-oxoglutarate, a required co-factor for its oxygenase activity [27]. EGL-9 regulates the response to iron depletion and hypoxia: in the presence of sufficient Fe^{2+} and oxygen, EGL-9 can hydroxylate HIF-1 (hypoxia-inducible factor 1), leading to its ubiquitination and degradation. When either Fe^{2+} or oxygen are unavailable, HIF-1 is stable and can bind DNA to regulate adaptive transcriptional responses [27–29]. It is surprising that all three *fat-2(wa17)* suppressor alleles affected precisely the same amino acid within EGL-9, and we surmise that a special property is conferred to EGL-9 by this specific mutation. For example, this mutant version of EGL-9 may be unable to inactivate HIF-1 by hydroxylation but still retain other important functions. In agreement with this interpretation, we found that the *egl-9(sa307)* null mutant cannot act as a *fat-2(wa17)* suppressor **(Fig 5F**).

One of the *fat-2(wa17)* suppressors corresponds to a splice acceptor mutation in the 5th intron of HIF-1, which would result in a frameshift after the first 413 amino acids if splicing instead occurs with the following 6th intron splice acceptor site (**Fig 5B**). This *hif-1(et69)* allele is dominant: heterozygosity for *hif-1(et69)/+* provides better *fat-2(wa17)* suppression than *hif-1(et69)/hif-1(et69)* homozygosity (**S2B Fig)**. This suggests that the *hif-1(et69)* allele is a gain-of-function allele, which may be because the frameshift occurs just after the first of potentially two prolines that are hydroxylated by EGL-9 when

oxygen and Fe^{2+} levels are sufficient [27]. This is also consistent with the observation that the *hif-1(ok2654)* null allele is not a *fat-2(wa17)* suppressor (**Fig 5G**). Usually, hydroxylation of the prolines P400 and P621 causes recruitment of a ubiquitin ligase leading to HIF-1 degradation [27]. In the case of the *hif-1(et69)* allele, such regulation is likely impossible, and a constitutive HIF-1 may act as a *fat-2(wa17)* suppressor in several ways: promote overexpression of lipid metabolism genes including *fat-2* [30], inhibit fatty acid beta-oxidation [31,32], which may help PUFAs to reach adequate levels even in the *fat-2(wa17)* mutant, or suppress the expression of the ferritin-encoding *ftn-2*, thus increasing the levels of ferrous ions required for desaturase activity [33,34].

Most informatively, the last two *fat-2(wa17)* suppressor mutations introduced premature STOP codons within the *ftn-2* gene (alleles *et67* and *et68*; **Fig 5B**). Additionally, the *ftn-2(ok404)* null allele also acted as a potent *fat-2(wa17)* suppressor (**Fig 5H**) which is consistent with inhibition of *ftn-2* being the key outome from HIF-1 pathway activation. *C. elegans ftn-2* encodes a ferritin that is expressed in intestine, muscle and several neurons [35]. The FTN-2 protein is constitutive and 10X faster as a ferroxidase (oxidising the reactive ferrous Fe^{2+} to the harmless ferric Fe^{3+}) than FTN-1, which is an inducible intestine-specific ferritin in *C. elegans* [33,36–39]. Additionally, FTN-2 is the major binder of iron in worms, and *ftn-2* mutants therefore contain much less iron than wild-type worms, though the Fe^{2+}/Fe^{3+} ratio is increased among the remaining iron [40]. This is likely the mechanism by which the *ftn-2(et67)* and *ftn-2(et68)* alleles act as *fat-2(wa17)* suppressors: increasing the availability of ferrous ions is a potent way to activate desaturases [34] and thus likely increases the activity of the near null *fat-2(wa17)* allele leading to the production of more/sufficient PUFAs. Importantly, the *ftn-2(et68)* allele was also able to suppress the growth defect resulting from *fat-2* knockdown (using RNAi; **Fig 5I**); this shows that ferritin mutations compensate for reduced *fat-2* activity generally rather than suppressing specifically only the *fat-2(wa17)* allele. Additionally, the *ftn-2(et68)* allele was not able to rescue the *fat-2(syb7458)* null allele (**S2C Fig)** suggesting that some *fat-2* activity must exist for *ftn-2(et68)* to act upon. Lastly, *ftn-2(et68)* is still a potent *fat-2(wa17)* suppressor when *hif-1* is knocked out (**S2D Fig**), suggesting that no other HIF-1-dependent functions are required as long as *ftn*-2 is downregulated; this conclusion is supported by the observation that the potency of the *ftn-2(ok404)* null allele to act as a *fat-2(wa17)* suppressor is not increased by including the *hif-1(et69)* allele (compare **Fig 5H and S2E Fig**). Altogether the genetic interaction studies suggests that the suppressor mutations in *ftn-2* and *hif-1* are acting via the same mechanism to rescue *fat-2(wa17)* and that *ftn-2* is downstream of *hif-1* in the *fat-2* suppression pathway.

Effect of *fat-2(wa17)* suppressors on HIF-1 and PUFA levels

The results of the *fat-2(wa17)* suppressor screen support a model where the *egl-9* R557 substitution alleles have an impaired ability to suppress HIF-1, while the gain-of-function *hif-1(et69)* allele

constitutively suppresses *ftn-2* expression and the *ftn-2* null alleles are unable to sequester ferrous ions of which elevated levels increase *fat-2* activity (**Fig 5C**). A 3xFLAG-tagged version of the endogenous HIF-1 allowed us to monitor HIF-1 levels in different conditions using Western blots (**Fig 6A-B**). As expected, hypoxia caused elevated levels of HIF-1 in wild-type worms. HIF-1 levels are abnormally low in *fat-2(wa17)* during normoxia but restored to normal levels by the internal *fat-2(et65)* mutation, suggesting that low PUFA levels cause HIF-1 downregulation. Nevertheless, HIF-1 levels are also increased by hypoxia in the *fat-2(wa17)* mutant indicating that the *hif-1* locus is still responsive to oxygen levels in the *fat-2(wa17)* mutant. As expected, *egl-9(et60)* drastically increases HIF-1 expression in *fat-2(wa17)*, which is consistent with the R557 substitution impairing the ability of EGL-9 to inhibit HIF-1. Finally, the null *ftn-2(et68)* allele caused near-loss (a faint HIF-1 band is occasionally seen) of detectable HIF-1 in *fat-2(wa17)*, suggesting feedback regulation between *ftn-2* and *hif-1* (**Fig 6A-B, S3A-B Fig**).

Inhibition of *egl-9* promotes HIF-1 activity [41], which we here verified for *the egl-9(et60*) allele using western blots **(Fig 6A)**. Additionally, we found by qPCR that *ftn-2* mRNA levels are as expected reduced by the proposed gain-of-function *hif-1(et69)* allele **(Fig 6C)**. We conclude that the *egl-9* and *hif-1* suppressor mutations likely converge on inhibiting *ftn-2* and thus act similarly to the *ftn-2* loss-of-function alleles.

We also used Western blots to evaluate the abundance of the FAT-2 protein expressed from endogenous wild-type or mutant loci but to which a HA tag was fused using CRISPR/Cas9. We found that the FAT-2::HA levels are severely reduced when the locus contains the S101F substitution present in the *wa17* allele, but restored close to wild-type levels by the *fat-2(et65)* suppressor mutation **(Fig 6D-E, S3C-D Fig)**. The levels of FAT-2 in the HIF-1 pathway suppressors varied between experiments, with the suppressors sometimes restoring FAT-2 levels and sometimes not even when the worms were growing well **(Fig 6D-E, S3C-D Fig)**. The *fat-2(wa17)* suppressors, except for the intragenic *fat-2* alleles, likely do not act by increasing FAT-2 protein levels.

As already mentioned, ferrous ions (Fe^{2+}) are potent activators of desaturases [34]. Given that each of the *fat-2(wa17)* suppressor mutants within the HIF-1 pathway are predicted to ultimately inhibit *ftn-2*, thus increasing the ferrous ion pool, we hypothesized that PUFA levels should be at least partially normalized in the *fat-2(wa17)* suppressors. This was confirmed by lipidomic analysis of phosphatidylcholines (**Fig 7A**) and phosphatidylethanolamines (**S4A Fig**). In particular, while levels of 18:2 (LA) were not significantly increased in the suppressor strains, the levels of 20:5 (EPA) were significantly increased by more than three folds and to levels near those obtained earlier by supplementing with LA (**Fig 7B-C, S4B-C Fig**), likely because the suppressor mutations allow *fat-*

2(wa17) to produce more LA that is converted by other elongases and desaturases into EPA, the end product.

Multiple stress response pathways are active in *fat-2(wa17)* and suppressed by *ftn-2(et68)*

The increase in EPA, and PUFA levels in general, likely explains the improved development and growth of *fat-2(wa17)*. We examined other traits that may be rescued by the *fat-2* suppressors, using the *ftn-2(et68)* mutant as representative because the *egl-9* and *hif-1* alleles converge on it. We found that the membrane fluidity defects in *fat-2(wa17)* were suppressed by *ftn-2(et68)* (**Fig 8A-C**). Additionally, several stress response pathways that are constitutively activated in the *fat-2(wa17)* mutant were also rescued by *ftn-2(et68)*. The mitochondrial UPR (visualized with a *hsp-60::GFP* reporter [42]) is activated in *fat-2(wa17)* at a level similar to that in *afts-1(et15)*, a known activator of mitochondrial stress [43], and this is suppressed by *ftn-2(et68)* (**Fig 8D-E**). Similarly, the metabolic stress reporter DAF-16::GFP [44] is constitutively nuclear-localized in *fat-2(wa17)* and this is also suppressed by *ftn-2(et68)* (**Fig 8F-G**). Using a *hsp-4::GFP* reporter [45], we found that the ER UPR is only slightly activated in *fat-2(wa17)* relative to WT (especially in spermatheca), and that this stress response too is partially suppressed by *ftn-2(et68)* (**Fig 8H-I**). Altogether, these results show that the PUFA-deficient *fat-2(wa17)* mutant engages multiple stress response pathways and that these are abated by *ftn-2(et68*).

Mimicking *fat-2(wa17)* suppressors using hypoxia or iron supplements

Attempts to mimic the effects of the *fat-2(wa17)* suppressor mutations by hypoxia or supplement treatments were only partially successful. Providing *fat-2(wa17)* with ferric ammonium citrate (FAC), which increases the levels of ferric ions that can be converted into ferrous ions as well as overall iron levels in worms [46], provided only a slight rescue of the *fat-2(wa17)* mutant (**Fig 9A**). Additionally, providing *fat-2(wa17)* with ferrous ions in the form of ferrous chloride did not provide any rescue (**S5A Fig)**. Reducing the levels of ferrous ions with the iron chelator deferoxamine, which we hypothesized would further hinder *fat-2(wa17)* growth, had no effect (**S5B Fig**); however, given that the *fat-2(syb7458)* null mutant grows at the same rate as *fat-2(wa17)* in 72 hours (**S5C Fig**) but never develops into an adult, we theorize that 72 hours may be too short to see a negative effect from deferoxamine on *fat-2(wa17)*. HIF-1-activating paraquat (PQ; [47]) likewise conferred only a small rescue (**Fig 9B**), while the combination of FAC and PQ did not provide any additional growth rescue, both at 20°C and 25°C (**Fig 9C; S5D Fig**). The HIF-1 activator hydrogen peroxide [48] also only mildly rescued *fat-2(wa17)* (**Fig 9D**), while two separate hypoxia mimetics (cobalt chloride [49] and sodium sulfite [50]) did not suppress the poor growth of *fat-2(wa17)* (**S5E-F Fig**). Additionally, exposing *fat-2(wa17)* to multiple short hypoxia treatments slightly increased growth, but longer hypoxia treatments had no effect (**Fig 9E**). Finally, we also tested a cocktail of eicosanoids, which are derived from PUFAs such as EPA and could be limiting in the *fat-2(wa17)* mutant, but found that they had no rescuing effect when added

as a supplement to the culture plates; their half-life and uptake by the worms are unknown (**S5G Fig**). Taken together, these results suggest that increasing iron and activating HIF-1 are beneficial to *fat-2(wa17)*, but that achieving physiologically optimal dosing via experimental treatments is difficult.

DISCUSSION

That dietary PUFAs are essential for mammalian health, with LA and ALA acting as precursors for the synthesis of other PUFAs, is known since the 1930s [9]. PUFAs have been linked to several important cellular and physiological processes (reviewed in [51–53]), including cell membrane properties and organelle dynamics (1,50), autophagy [54], mitochondria function [55], ferroptosis [56–58], regulation of the *daf-2/*insulin, mTOR and p38-MAPK pathways [59–61], SREBP stability and signaling [62,63], lipid droplet fusion [64], neuronal signaling and neurotransmission [65–67], TRPV-dependent sensory signaling [65], oocyte development [68], and telomere length [69]. Which of these, if any, is the specific essential role of PUFAs in animal physiology? And are there molecular mechanisms that can compensate for PUFA deficiency? In the present study we approached these questions using forward genetics in *C. elegans*. While *C. elegans* can *de novo* synthesize PUFAs, mutations that impair the production of certain PUFAs can lead to developmental defects or lethality [10,19,70], offering opportunities for suppressor screens. Here, we showed that defects in the *fat-2(wa17)* mutant, which has limited Δ12 desaturase activity and only produces trace amounts of PUFAs, are suppressed by either compensatory intragenic mutations within *fat-2* itself or by mutations within the HIF-1 pathway. The fact that screening approximately 40 000 haploid genomes for *fat-2(wa17)* suppressors and finding mutations only within *fat-2* itself or within the HIF-1 pathway suggests that the screen has reached near-saturation and that we may have identified most, if not all, possible genetic ways to compensate for the *fat-2(wa17)* mutation. Importantly, none of the *fat-2(wa17)* suppressor mutations that we identified compensate for the PUFA shortage itself. Instead, the *fat-2(wa17)* suppressors act by boosting desaturase activity to allow the *fat-2(wa17)* mutant to synthesize more PUFAs; the *fat-2(wa17)* suppressors therefore cannot suppress the defects of the *fat-2* null mutant, as we specifically showed for *ftn-2(et68)*. We draw the important conclusion that PUFAs are not only essential but also that their essential functions cannot be genetically replaced.

The *fat-2(wa17)* suppressor mutations within the HIF-1 pathway converge on the inhibition of *ftn-2*. The primary function of ferritin is to provide a harmless storage of iron within cells: ferritin promotes the oxidation of ferrous ions and stores the resulting ferric ions in a mineralized form [71]. Thus *ftn-2* inhibition results in reduced total cellular iron but increased levels of ferrous ions, i.e. Fe^{2+} [72,73]. Importantly, ferrous ions are required for desaturase reactions and increasing ferrous ion concentration is a potent way to increase activity because it accelerates the rate at which the desaturase cycles from the inactive post-reaction Fe^{3+}-bound state to the active Fe^{2+}-bound state [34,74]. Because eukaryotic

desaturases are all evolutionarily closely related [75] and act in essentially the same way, ferrous ions must also be potent FAT-2 activators and thus boost the output from the mutant FAT-2(S101F) protein produced by the *fat-2(wa17)* allele or from the reduced FAT-2 protein levels in *fat-2* RNAi-treated worms. Our findings suggest an elegant explanation for the observation that HIF-1 inhibits *ftn-2* expression in *C. elegans* [33]: this is likely an adaptive response to boost desaturase activity when oxygen or iron is limiting, insuring a maximum output under adverse conditions. Fe^{2+} and HIF may contribute to desaturase boost also in human since CytB5 (which supplies Fe^{2+} to desaturases) promotes SFA tolerance while VHL (which causes HIF degradation) prevents SFA tolerance in cultured cells [76]. Other mechanisms are also possible. For example, mutations in the HIF-1 pathway could somehow reduce EPA turnover rates in the *fat-2(wa17)* mutant and allow its levels to rise above an essential threshold. This hypothesis is consistent with the observation that the suppressors can rescue both the *fat-2(wa17)* mutant and *fat-2* RNAi-treated worms but not the *fat-2* null mutant. It is even possible, though deemed unlikely, that the *fat-2(wa17)* suppressors act by compensating for the PUFA shortage via some undefined separate process downstream of the lipid changes and that they only indirectly result in elevated EPA levels.

Lipidomic analysis showed that among all PUFAs, it was the EPA levels that were best restored by the *fat-2(wa17)* suppressors. It is likely that any LA molecule produced in the mutants is quickly acted upon by downstream desaturases and elongases, leading to increased levels of the end product, namely EPA. EPA may be a sufficient or particularly important PUFA for sustaining *C. elegans* health given that the *fat-2(wa17)* mutant is well rescued by EPA supplements. Indeed, DHA, which is not produced by *C. elegans*, is also able to rescue the *fat-2(wa17)* mutant. Others have shown that supplementing nearly completely EPA-deficient *fat-3 C. elegans* mutants with DHA significantly restored their EPA levels, suggesting that DHA supplements reduce EPA turnover [77]. EPA and DHA, being long chain PUFAs should have similar fluidizing effects on membrane properties (though in *vitro* experiments challenge this view [78]), and both can serve as precursors of eicosanoids or docosanoids, particularly inflammatory ones [79]. Abundant literature indicates that EPA is a particularly important PUFA in *C. elegans*. Phosphatidylcholines containing two attached EPA molecules are very abundant in *C. elegans* membranes, and their abundance increases the most in response to a temperature shift from 25°C to 15°C, suggesting an important role in fluidity homeostasis [80]. Long chain PUFAs such as EPA are required for efficient neurotransmission in *C. elegans*: mutants unable to produce them have depleted levels of synaptic vesicles accompanied by poor motility and these defects are rescued by exogenous PUFAs, including DHA [77]. *C. elegans* can also convert EPA to eicosanoids in a cytochrome P450-dependent manner [81,82]; inhibiting this process results in reduced pharyngeal pumping rate suggesting that regulation of muscular contraction by eicosanoids is conserved from nematodes to mammals [83]. EPA-derived eicosanoids are also required for guiding some cell migrations in *C. elegans*, including that of sperm [84]. EPA, and other PUFAs, can inhibit the nuclear localization of

DAF-16 in *fat-2*-RNAi-treated worms, suggesting that they mediate signaling via this insulin receptor homolog and thus generally promote growth in *C. elegans* rather than stress resistance and fat storage [59]. In conclusion, EPA is clearly an important PUFA in *C. elegans* and our work suggests that its multifaceted functions cannot be replaced by mutations in any one gene.

Finally, the case of the three novel *egl-9* alleles isolated in our screen deserves special attention. All three alleles specifically affect the arginine at position 557 of the EGL-9 protein (it is converted to a histidine in two of the alleles, and to a cysteine in the third). This Arg557 in EGL-9 is specifically required for its ability to hydroxylate HIF-1 thus marking it for ubiquitin-dependent degradation [27]. Null alleles of *egl-9* were not picked in our screen and directly testing such a null allele revealed it to be ineffective as a *fat-2(wa17)* suppressor. We conclude that the EGL-9 proteins bearing a mutation at position Arg557 retain important functions while being unable to hydroxylate HIF-1. Others have previously demonstrated that EGL-9 could inhibit HIF-1 even when unable to hydroxylate it [41]. Clearly there is more to EGL-9 than its function as a HIF-1 hydroxylase and it would be interesting in the future to detail this further.

We conclude that PUFA-deficient *fat-2(wa17)* mutants benefit only slightly from membrane-fluidizing treatments, that there is likely no genetic way to compensate for PUFA deficiency. *fat-2(wa17)* mutants can only be rescued by boosting the activity of its defective desaturase, and restoring EPA levels are likely sufficient to suppress most *fat-2(wa17)* phenotypes suggesting a particularly important role for this PUFA in *C. elegans.* In the future it will be interesting to determine if boosting desaturase activity by inhibition of ferritin expression via HIF-1 is also a beneficial response to hypoxia in worms and human.

MATERIALS AND METHODS

C. elegans strains and cultivation

The wild-type C. elegans reference strain N2, *fat-2(wa17), nhr-49(et8), mdt-15(et14), paqr-1(et52), paqr-2(3410), acs-13(et54), fld-1(et46), hif-1(ok2564), ftn-2(ok404), ftn-1(ok3625), egl-9(sa307), atfs-1(et15), zcIs4 [hsp-4::GFP], zcIs9 [hsp-60::GFP + lin-15(+)]* and *zIs356 [daf-16p::daf-16a/b::GFP + rol-6(su1006)]* are available from the *C. elegans* Genetics Center (CGC; USA). The PHX7548 (*fat-2(syb7458)/nT1[qIs51]*(IV;V)) strain was created by Suny Biotech Co using CRISPR/Cas9 and carries a deletion of 1387bp between flanking sequences 5'-aaacttggcccccgacgaagatg-3' and 5'-gtgataatgacgagaataagtcct-3'. *fat-2(syb7458)* worms were maintained in an unbalanced state on non-peptone plates containing OP50 grown overnight in LB containing 2 mM linoleic acid.

Unless otherwise stated, experiments were performed at 20°C, using the *E. coli* strain OP50 as a food source, which was re-streaked every 6-8 weeks and maintained on LB plates at 4°. Single colonies were

cultivated overnight at 37°C in LB medium before being used to seed NGM plates. Stock solutions of supplements were filter-sterilized and added to cooled NGM after autoclaving to produce supplement plates.

Construction of *fat-2(+)*

The *pfat-2(+)* construct was generated with the NEB PCR Cloning Kit for amplification of *fat-2(+)* with the following primers: 5'-gagctcaagaagcgtttcca-3' and 5'-gggcaagaatttgtagtgtca-3' using N2 genomic DNA. Plasmids were prepared with a GeneJet Plasmid Miniprep Kit and injected at the following concentrations: *pfat-2(+)* of 20 µg/µl, *pRF4(rol-6)* of 40 µg/µl, and *pBSKS* of 35 µg/µl into *fat-2(wa17)* and N2 worms.

Pre-loading of *E. coli* with fatty acids or eicosanoids

Stock solutions of fatty acids (Merck) or eicosanoids (Primary Eicosanoid HPLC Mixture; Cayman Chemical) dissolved in ethanol (EPA, DHA, OA), DMSO (LA), or methyl acetate (eicosanoids) were diluted in LB media to the appropriate final concentration, inoculated with OP50 bacteria, and shaken overnight at 37°C. The bacteria were washed twice in M9 to remove fatty acids, concentrated 10X by centrifugation, dissolved in LB and seeded onto NGM plates lacking peptone.

Growth assays

For length measurement studies, synchronized L1s were plated onto test plates seeded with OP50 and worms were mounted and photographed 72 h later. Experiments performed at 15°C were photographed after 144 h. The length of 20 worms was measured using ImageJ.

For hydrogen peroxide treatment, synchronized worms were incubated in 2 mM hydrogen peroxide for 2 h at L1 stage before being plated on NGM plates for 72 h. For hypoxia treatment, synchronized L1s were incubated for 2-6 h in a hypoxia chamber, returned to normoxia for 24h, and hypoxia exposure was repeated as stated in the figure.

Oil Red O staining

Synchronized day 1 adults were washed three times with PBST and fixed for 3 minutes in 60% isopropanol. Worms were then rotated for 2 h in filtered 60% Oil Red O staining solution. The stained worms were washed three times in PBST before being mounted on agarose pads and imaged with a Zeiss Axioscope microscope.

Mutagenesis and screen for *fat-2(wa17)* suppressors

fat-2(wa17) worms were mutagenized for 4 hours by incubation in the presence of 0.05 M ethyl methane sulfonate (EMS) according to the standard protocol [85]. The worms were then washed and spotted

onto an NGM plate. After 2 h, L4 hermaphrodite animals were transferred to new plates. 8-10 days later, F1 progeny were bleached, washed, and their eggs allowed to hatch overnight in M9. The resulting L1 larvae were spotted onto new plates, cultivated at 20°C, then screened after 72 h for gravid F2 worms, which were then picked to new plates for further analysis. In total, approximately 40 000 independently mutagenized haploid genomes were screened. The isolated suppressor mutants were outcrossed 4 to 6 times prior to whole genome sequencing, and 8 to 10 times prior to characterization. Outcrossing was done by mating N2 males to a suppressor, then crossing male progeny to *fat-2(wa17)* mutant worms. Progeny from this cross were picked to individual plates and kept at 20°C then screened for *fat-2(wa17)* homozygosity using PCR, followed by testing the F2 progeny for ability to grow to adults in 72 h. Genotyping primers for the suppressor mutants are included in **S1 Table**.

Whole genome sequencing

The genomes of the ten suppressor mutants that had been outcrossed 4 or 6 times were sequenced by Eurofins (Constance, Germany) with a mean coverage varying from 40.68X to 63.05X and their genomes assembled using the *C. elegans* genome version cel235 from Ensembl (REF: PMID: 37953337). Eurofins applied customised filters to the variants to filter false positives using GATK's Variant Filtration module [86,87]. Variants detected were annotated based on their gene context using snpEff [88]. For each suppressor mutant, one or two hot spots, i.e. small genomic area containing several mutations, were identified and candidate mutations tested experimentally as described in the text.

CRISPR-Cas9 genome editing

The recreation of the candidate suppressor mutations and insertion of the 3xFLAG tag into the *hif-1* gene was performed using CRISPR-Cas9 gene editing as previously described [89,90]. The insertion of the ssDNA oligos was performed utilizing the homology-direct repair (HDR) mechanisms. The protospacer-adjacent motif (PAM) site of the ssDNA oligo template was flanked by 40 bp homology arms. Design and synthesis of the ssDNA and CRISPR RNA (crRNA) was performed using the Alt-R HDR Design Tool from IDT (Integrated DNA Technologies, Inc.; Coralville, IA, USA), including proprietary modifications that improve oligo stability. To recreate the *hif-1(et69)* allele, we used the crRNA sequence 5'- UUUCUUAACGUGUGUAUUUCGUUUUAGAGCUAUGCU-3' and the DNA oligo donor sequence 5'-AGTTCCATACATTTAGCAAGTGATTTCTTAACGTGTGTATTTCAAGAGCACGTAAGAACAGCTACGATGACGTTTTGCAATGGCT-3. To introduce the 3xFLAG at the N-terminus coding end of *hif-1* we used the crRNA sequence 5'-GAAAAUAAUCAAGAGAGCAUGUUUUAGAGCUAUGCU-3' and the DNA oligo donor sequence 5'-AAATGAACAACAGCCTAGTTCTTATTCCCCATTTCCAATGCTCTCTGACTACAAGGACCA

CGACGGCGATTATAAGGATCACGACATCGACTACAAAGACGACGATGACAAGTGATTAT TTTCTACCCCCTCTCAAACTGTTCATTGTTTTG-3'. The injection mixes were prepared using 10 µg/µl of the Cas9 enzyme (IDT), 0.4 µg/µl tracrRNA (IDT), 2.8 0.4 µg/µl crRNA (IDT), 1 µg/µl of ssDNA (IDT), and 40 ng/µl of PRF4(*rol-6*) or Pmyo-2(GFP) plasmid. The mixture was microinjected into the posterior gonad of the worm and the F1 generation was screened for animals expressing the reporter plasmid. Genotypes were tested by PCR and successfully edited genes were confirmed by Sanger sequencing (Eurofins).

Fluorescence recovery after photobleaching (FRAP)

FRAP experiments were carried out using a membrane-associated prenylated GFP reporter expressed in intestinal cells as previous described [91], using a Zeiss LSM700inv laser scanning confocal microscope with a 40X water immersion objective. Briefly, the GFP positive membranes were photobleached over a rectangular area (30 x 4 -pixels) using 30 iterations of the 488 nm laser with 50% laser power transmission. Images were collected at a 12-bit intensity resolution over 256 x 256 pixels (digital zoom 4X) using a pixel dwell time of 1.58 µs, and were all acquired under identical settings. The recovery of fluorescence was traced for 25 seconds. Fluorescence recovery and T_{half} were calculated as previously described [18].

Stress Response Assay

Worms were imaged with a Zeiss Axioscope and fluorescence intensity was quantified with ImageJ (n≥20 for all experiments). Worm strains carrying *hsp-60::GFP* were imaged as day 1 adults, and the fluorescence values were taken from a 39 µm circumference circle in the brightest part of the anterior part of the worm. Worm strains carrying *DAF-16::GFP* were imaged as L4s and the percentage of worms with cytoplasmic or nuclear localization was quantified. Worm strains carrying *hsp-4::GFP* were imaged as day 1 adults and the fluorescence of the whole worm was quantified.

Lipidomics

Samples were composed of synchronized L4 larvae (one 9 cm diameter plate/sample; each treatment/genotype was prepared in four independently grown replicates) grown on NGM or non-peptone plates seeded with linoleic acid. In the case of LA to NGM samples, worms were grown until late L3/early L4 stage on linoleic acid seeded non-peptone plates before being transferred to NGM plates for 6 h before collection. Worms were washed 3 times in M9, pelleted and stored at -80°C until analysis. For lipid extraction, the pellet was sonicated for 10 minutes in methanol;butanol [1:3] and then extracted according to published methods [92]. Lipid extracts were evaporated and reconstituted in chloroform:methanol [1:2] with 5 mM ammonium acetate. This solution was infused directly (shotgun approach) into a QTRAP 5500 mass spectrometer (Sciex) equipped with a TriVersa NanoMate (Advion Bioscience) as described previously [93]. Phospholipids were measured using precursor ion scanning

in negative mode using the fatty acids as fragments [94,95]. To generate the phospholipid composition (as mol%) the signals from individual phospholipids (area under the m/z peak in the spectra) were divided by the signal from all detected phospholipids of the same class. The data were evaluated using the LipidView software (Sciex). The data were further analyzed using Qlucore Omics Explorer n.n (Qlucore AB) for analysis. The data were normalized for the purpose of the heat map visualization (mean = 0; variance = 1).

Protein extraction and western blots

Worms were lysed using lysis buffer containing 25 mM Tris (pH 7.5), 300 mM NaCl, 0.1% NP40, and 1X protease inhibitor on ice with a motorized pestle. Samples were centrifuged at 20000g for 15 min at 4°C and protein sample concentration was quantified using BCA protein assay kit. 15 µg of protein were mixed with Laemmli sample loading buffer contained β-mercaptoethanol, boiled for 10 min, and loaded in 4% to 20% gradient precast SDS gel. After electrophoresis, the proteins were transferred to nitrocellulose membranes using Trans-Blot Turbo Transfer Packs and a Trans-Blot Turbo apparatus/predefined mixed-MW program. Blots were blocked in 5% nonfat dry milk in PBST for 1 h at room temperature. Blots were incubated with primary antibodies overnight at 4°C (mouse monoclonal anti-FLAG antibody (M2, Sigma Aldrich) 1:5000 dilution) or 1 h at room temperature (mouse monoclonal anti-alpha-Tubulin (B512, Sigma Aldrich) 1:5000 dilution). Blots were then washed with PBST and incubated with swine-anti rabbit HRP 1:3000 dilution or goat anti-mouse HRP 1:3000 dilution for 1 h at room temperature and washed again with PBST. Detection of the hybridized antibody was performed using and ECL detection kit (Immobilon Western, Millipore), and the signal was visualized with a digital camera (VersaDoc, Bio-Rad).

Quantitative PCR (qPCR)

Total cellular worm RNA was isolated using RNeasy Plus Kit according to the manufacturer's instructions (Qiagen) and quantified using a NanoDrop spectrophotometer (ND-1000; Thermo Scientific). cDNA was obtained using the RevertAid H Minus First Strand cDNA Synthesis Kit (Thermo Scientific) with random hexamers. qPCR was performed with a CFX Connect thermal cycler (Bio-Rad) using HOT FIREpol EvaGreen qPCR SuperMix (Solis Biodyne) and standard primers. Samples were measured as triplicates. The relative expression of each gene was calculated according to the delta-delta CT method. Expression of the housekeeping gene *tba-1* was used to normalize for variations in RNA input. Primers used were as follows: *ftn-2*, forward (TACCACTCCGAGGTTGAAGC) and reverse (TGGAAGGGCAACATCGTCAC); *tba-1*, forward (TCTCGCAGGTTGTGTCTTCC) and reverse (AGCCTCATGGTAAGCCTGAA).

Statistics

Error bars for the worm length measurements show the standard error of the mean, and one-way ANOVA tests were used to identify significant differences from *fat-2(wa17)* control unless otherwise stated. All experiments were independently repeated at least twice with similar results, and the statistics shown apply to the presented experimental results.

ACKNOWLEDGEMENTS

Some strains were provided by the CGC, which is funded by NIH Office of Research Infrastructure Programs (P40 OD010440). This research was funded by Cancerfonden (22 1984 Pj) and Vetenskapsrådet (2024-04012).

REFERENCES

1. Barelli H, Antonny B. Lipid unsaturation and organelle dynamics. Curr Opin Cell Biol. 2016;41: 25–32. doi:10.1016/J.CEB.2016.03.012

2. Antonny B, Vanni S, Shindou H, Ferreira T. From zero to six double bonds: phospholipid unsaturation and organelle function. Trends Cell Biol. 2015;25: 427–436. doi:10.1016/J.TCB.2015.03.004

3. Bazinet RP, Layé S. Polyunsaturated fatty acids and their metabolites in brain function and disease. Nature Reviews Neuroscience 2014 15:12. 2014;15: 771–785. doi:10.1038/nrn3820

4. Simopoulos AP. Essential fatty acids in health and chronic disease. Am J Clin Nutr. 1999;70: 560s–569s. doi:10.1093/AJCN/70.3.560S

5. James MJ, Gibson RA, Cleland LG. Dietary polyunsaturated fatty acids and inflammatory mediator production. Am J Clin Nutr. 2000;71: 343s–348s. doi:10.1093/AJCN/71.1.343S

6. Bell M V., Henderson RJ, Sargent JR. The role of polyunsaturated fatty acids in fish. Comparative Biochemistry and Physiology -- Part B: Biochemistry and. 1986;83: 711–719. doi:10.1016/0305-0491(86)90135-5

7. Ruiz M, Devkota R, Kaper D, Ruhanen H, Busayavalasa K, Radović U, et al. AdipoR2 recruits protein interactors to promote fatty acid elongation and membrane fluidity. Journal of Biological Chemistry. 2023;299: 104799. doi:10.1016/J.JBC.2023.104799

8. Murff HJ, Edwards TL. Endogenous Production of Long-Chain Polyunsaturated Fatty Acids and Metabolic Disease Risk. Curr Cardiovasc Risk Rep. 2014;8: 1–9. doi:10.1007/S12170-014-0418-1/FULLTEXT.HTML

9. Burr GO, Burr MM. ON THE NATURE AND RÔLE OF THE FATTY ACIDS ESSENTIAL IN NUTRITION. Journal of Biological Chemistry. 1930;86: 587–621. doi:10.1016/S0021-9258(20)78929-5

10. Watts JL, Browse J. Genetic dissection of polyunsaturated fatty acid synthesis in Caenorhabditis elegans. Proc Natl Acad Sci U S A. 2002;99: 5854–5859. doi:10.1073/PNAS.092064799/ASSET/836784B8-935E-4A14-872C-DAD705337373/ASSETS/GRAPHIC/PQ0920647004.JPEG

11. Ichi I, Kono N, Arita Y, Haga S, Arisawa K, Yamano M, et al. Identification of genes and pathways involved in the synthesis of Mead acid (20:3n − 9), an indicator of essential fatty acid deficiency. Biochimica et Biophysica Acta (BBA) - Molecular and Cell Biology of Lipids. 2014;1841: 204–213. doi:10.1016/J.BBALIP.2013.10.013

12. Nakamura MT, Nara TY. Structure, function, and dietary regulation of delta6, delta5, and delta9 desaturases. Annu Rev Nutr. 2004;24: 345–376. doi:10.1146/ANNUREV.NUTR.24.121803.063211

13. Guillou H, Zadravec D, Martin PGP, Jacobsson A. The key roles of elongases and desaturases in mammalian fatty acid metabolism: Insights from transgenic mice. Prog Lipid Res. 2010;49: 186–199. doi:10.1016/J.PLIPRES.2009.12.002

14. Zhang JY, Kothapalli KSD, Brenna JT. Desaturase and elongase-limiting endogenous long-chain polyunsaturated fatty acid biosynthesis. Curr Opin Clin Nutr Metab Care. 2016;19: 103–110. doi:10.1097/MCO.0000000000000254

15. Peyou-Ndi MM, Watts JL, Browse J. Identification and characterization of an animal delta(12) fatty acid desaturase gene by heterologous expression in Saccharomyces cerevisiae. Arch Biochem Biophys. 2000;376: 399–408. doi:10.1006/ABBI.2000.1733

16. Zhou XR, Green AG, Singh SP. Caenorhabditis elegans Δ12-Desaturase FAT-2 Is a Bifunctional Desaturase Able to Desaturate a Diverse Range of Fatty Acid Substrates at the Δ12 and Δ15 Positions. Journal of Biological Chemistry. 2011;286: 43644–43650. doi:10.1074/JBC.M111.266114

17. Svensk E, Ståhlman M, Andersson CH, Johansson M, Borén J, Pilon M. PAQR-2 Regulates Fatty Acid Desaturation during Cold Adaptation in C. elegans. PLoS Genet. 2013;9: e1003801. doi:10.1371/JOURNAL.PGEN.1003801

18. Svensk E, Devkota R, Ståhlman M, Ranji P, Rauthan M, Magnusson F, et al. Caenorhabditis elegans PAQR-2 and IGLR-2 Protect against Glucose Toxicity by Modulating Membrane Lipid Composition. PLoS Genet. 2016;12: e1005982. doi:10.1371/JOURNAL.PGEN.1005982

19. Dancy BCR, Chen SW, Drechsler R, Gafken PR, Olsen CP. 13C- and 15N-labeling strategies combined with mass spectrometry comprehensively quantify phospholipid dynamics in C. elegans. PLoS One. 2015;10: 1–23. doi:10.1371/journal.pone.0141850

20. Tanaka T, Ikita K, Ashida T, Motoyama Y, Yamaguchi Y, Satouchi K. Effects of growth temperature on the fatty acid composition of the free-living nematodeCaenorhabditis elegans. Lipids. 1996;31: 1173–1178. doi:10.1007/BF02524292

21. Devkota R, Kaper D, Bodhicharla R, Henricsson M, Borén J, Pilon M. A genetic titration of membrane composition in Caenorhabditis elegans reveals its importance for multiple cellular and physiological traits. Genetics. 2021;219. doi:10.1093/GENETICS/IYAB093

22. Devkota R, Svensk E, Ruiz M, Ståhlman M, Borén J, Pilon M. The adiponectin receptor AdipoR2 and its Caenorhabditis elegans homolog PAQR-2 prevent membrane rigidification by exogenous saturated fatty acids. PLoS Genet. 2017;13: e1007004. doi:10.1371/JOURNAL.PGEN.1007004

23. Hutzell PA, Krusberg LR. Fatty acid compositions of Caenorhabditis elegans and C. Briggsae. Comparative Biochemistry and Physiology Part B: Comparative Biochemistry. 1982;73: 517–520. doi:10.1016/0305-0491(82)90068-2

24. Ruiz M, Bodhicharla R, Svensk E, Devkota R, Busayavalasa K, Palmgren H, et al. Membrane fluidity is regulated by the C. Elegans transmembrane protein FLD-1 and its human homologs TLCD1/2. Elife. 2018;7. doi:10.7554/ELIFE.40686

25. Ruiz M, Bodhicharla R, Ståhlman M, Svensk E, Busayavalasa K, Palmgren H, et al. Evolutionarily 1 conserved long-chain acyl-coa synthetases regulate membrane composition and fluidity. Elife. 2019;8. doi:10.7554/eLife.47733

26. Busayavalasa K, Ruiz M, Devkota R, Ståhlman M, Bodhicharla R, Svensk E, et al. Leveraging a gain-of-function allele of Caenorhabditis elegans paqr-1 to elucidate

membrane homeostasis by PAQR proteins. PLoS Genet. 2020;16: e1008975. doi:10.1371/journal.pgen.1008975

27. Epstein ACR, Gleadle JM, McNeill LA, Hewitson KS, O'Rourke J, Mole DR, et al. C. elegans EGL-9 and Mammalian Homologs Define a Family of Dioxygenases that Regulate HIF by Prolyl Hydroxylation. Cell. 2001;107: 43–54. doi:10.1016/S0092-8674(01)00507-4

28. Bracken CP, Fedele AO, Linke S, Balrak W, Lisy K, Whitelaw ML, et al. Cell-specific regulation of hypoxia-inducible factor (HIF)-1alpha and HIF-2alpha stabilization and transactivation in a graded oxygen environment. J Biol Chem. 2006;281: 22575–22585. doi:10.1074/JBC.M600288200

29. Huang LE, Arany Z, Livingston DM, Franklin Bunn H. Activation of Hypoxia-inducible Transcription Factor Depends Primarily upon Redox-sensitive Stabilization of Its α Subunit. Journal of Biological Chemistry. 1996;271: 32253–32259. doi:10.1074/JBC.271.50.32253

30. Xie M, Roy R. Increased Levels of Hydrogen Peroxide Induce a HIF-1-dependent Modification of Lipid Metabolism in AMPK Compromised C. elegans Dauer Larvae. Cell Metab. 2012;16: 322–335. doi:10.1016/J.CMET.2012.07.016

31. Huang D, Li T, Li X, Zhang L, Sun L, He X, et al. HIF-1-mediated suppression of acyl-CoA dehydrogenases and fatty acid oxidation is critical for cancer progression. Cell Rep. 2014;8: 1930–1942. doi:10.1016/J.CELREP.2014.08.028

32. Papandreou I, Cairns RA, Fontana L, Lim AL, Denko NC. HIF-1 mediates adaptation to hypoxia by actively downregulating mitochondrial oxygen consumption. Cell Metab. 2006;3: 187–197. doi:10.1016/J.CMET.2006.01.012

33. Romney SJ, Newman BS, Thacker C, Leibold EA. HIF-1 Regulates Iron Homeostasis in Caenorhabditis elegans by Activation and Inhibition of Genes Involved in Iron Uptake and Storage. PLoS Genet. 2011;7: e1002394. doi:10.1371/JOURNAL.PGEN.1002394

34. Shen J, Wu G, Pierce BS, Tsai AL, Zhou M. Free ferrous ions sustain activity of mammalian stearoyl-CoA desaturase-1. Journal of Biological Chemistry. 2023;299. doi:10.1016/j.jbc.2023.104897

35. Romney SJ, Thacker C, Leibold EA. An Iron Enhancer Element in the FTN-1 Gene Directs Iron-dependent Expression in Caenorhabditis elegans Intestine. Journal of Biological Chemistry. 2008;283: 716–725. doi:10.1074/JBC.M707043200

36. Kim Y Il, Cho JH, Yoo OJ, Ahnn J. Transcriptional Regulation and Life-span Modulation of Cytosolic Aconitase and Ferritin Genes in C. elegans. J Mol Biol. 2004;342: 421–433. doi:10.1016/J.JMB.2004.07.036

37. Romero-Afrima L, Zelmanovich V, Abergel Z, Zuckerman B, Shaked M, Abergel R, et al. Ferritin is regulated by a neuro-intestinal axis in the nematode Caenorhabditis elegans. Redox Biol. 2020;28: 101359. doi:10.1016/J.REDOX.2019.101359

38. Mubarak SSM, Malcolm TR, Brown HG, Hanssen E, Maher MJ, McColl G, et al. Biochemical Characterization of Caenorhabditis elegans Ferritins. Biochemistry. 2023;62: 1484–1496. doi:10.1021/ACS.BIOCHEM.3C00005/ASSET/IMAGES/LARGE/BI3C00005_0011.JPEG

39. Cha'on U, Valmas N, Collins PJ, Reilly PEB, Hammock BD, Ebert PR. Disruption of iron homeostasis increases phosphine toxicity in Caenorhabditis elegans. Toxicol Sci. 2007;96: 194–201. doi:10.1093/TOXSCI/KFL187

40. James SA, Roberts BR, Hare DJ, De Jonge MD, Birchall IE, Jenkins NL, et al. Direct in vivo imaging of ferrous iron dyshomeostasis in ageing Caenorhabditis elegans. Chem Sci. 2015;6: 2952–2962. doi:10.1039/C5SC00233H

41. Shao Z, Zhang Y, Powell-Coffman JA. Two Distinct Roles for EGL-9 in the Regulation of HIF-1-Mediated Gene Expression in Caenorhabditis elegans. Genetics. 2009;183: 821. doi:10.1534/GENETICS.109.107284

42. Yoneda T, Benedetti C, Urano F, Clark SG, Harding HP, Ron D. Compartment-specific perturbation of protein handling activates genes encoding mitochondrial chaperones. J Cell Sci. 2004;117: 4055–4066. doi:10.1242/JCS.01275

43. Rauthan M, Ranji P, Pradenas NA, Pitot C, Pilon M. The mitochondrial unfolded protein response activator ATFS-1 protects cells from inhibition of the mevalonate pathway. Proc Natl Acad Sci U S A. 2013;110: 5981–5986. doi:10.1073/PNAS.1218778110/SUPPL_FILE/PNAS.201218778SI.PDF

44. Libina N, Berman JR, Kenyon C. Tissue-Specific Activities of C. elegans DAF-16 in the Regulation of Lifespan. Cell. 2003;115: 489–502. doi:10.1016/S0092-8674(03)00889-4

45. Calfon M, Zeng H, Urano F, Till JH, Hubbard SR, Harding HP, et al. IRE1 couples endoplasmic reticulum load to secretory capacity by processing the XBP-1 mRNA. Nature 2002 415:6867. 2002;415: 92–96. doi:10.1038/415092A

46. Valentini S, Cabreiro F, Ackerman D, Alam MM, Kunze MBA, Kay CWM, et al. Manipulation of in vivo iron levels can alter resistance to oxidative stress without affecting ageing in the nematode C. elegans. Mech Ageing Dev. 2012;133: 282. doi:10.1016/J.MAD.2012.03.003

47. Hwang AB, Ryu EA, Artan M, Chang HW, Kabir MH, Nam HJ, et al. Feedback regulation via AMPK and HIF-1 mediates ROS-dependent longevity in Caenorhabditis elegans. Proc Natl Acad Sci U S A. 2014;111: E4458–E4467. doi:10.1073/PNAS.1411199111/SUPPL_FILE/PNAS.1411199111.SD01.XLS

48. Xie M, Roy R. Increased Levels of Hydrogen Peroxide Induce a HIF-1-dependent Modification of Lipid Metabolism in AMPK Compromised C. elegans Dauer Larvae. Cell Metab. 2012;16: 322–335. doi:10.1016/J.CMET.2012.07.016

49. Padmanabha D, Padilla PA, You YJ, Baker KD. A HIF-independent mediator of transcriptional responses to oxygen deprivation in Caenorhabditis elegans. Genetics. 2015;199: 739–748. doi:10.1534/GENETICS.114.173989/-/DC1

50. Jiang B, Ren C, Li Y, Lu Y, Li W, Wu Y, et al. Sodium sulfite is a potential hypoxia inducer that mimics hypoxic stress in Caenorhabditis elegans. Journal of Biological Inorganic Chemistry. 2011;16: 267–274. doi:10.1007/S00775-010-0723-1/FIGURES/4

51. Calder PC. Mechanisms of action of (n-3) fatty acids. J Nutr. 2012;142. doi:10.3945/JN.111.155259

52. Vrablik TL, Watts JL. Polyunsaturated fatty acid derived signaling in reproduction and development: insights from Caenorhabditis elegans and Drosophila melanogaster. Mol Reprod Dev. 2013;80: 244–259. doi:10.1002/MRD.22167

53. Harayama T, Shimizu T. Roles of polyunsaturated fatty acids, from mediators to membranes. J Lipid Res. 2020;61: 1150. doi:10.1194/JLR.R120000800

54. O'Rourke EJ, Kuballa P, Xavier R, Ruvkun G. ω-6 Polyunsaturated fatty acids extend life span through the activation of autophagy. Genes Dev. 2013;27: 429. doi:10.1101/GAD.205294.112

55. Stanley WC, Khairallah RJ, Dabkowski ER. Update on lipids and mitochondrial function: impact of dietary n-3 polyunsaturated fatty acids. Curr Opin Clin Nutr Metab Care. 2012;15: 122. doi:10.1097/MCO.0B013E32834FDAF7

56. Yang WS, Kim KJ, Gaschler MM, Patel M, Shchepinov MS, Stockwell BR. Peroxidation of polyunsaturated fatty acids by lipoxygenases drives ferroptosis. Proc Natl Acad Sci U S A. 2016;113: E4966–E4975. doi:10.1073/PNAS.1603244113

57. Lee JY, Nam M, Son HY, Hyun K, Jang SY, Kim JW, et al. Polyunsaturated fatty acid biosynthesis pathway determines ferroptosis sensitivity in gastric cancer. Proc Natl Acad Sci U S A. 2020;117: 32433–32442. doi:10.1073/PNAS.2006828117

58. Perez MA, Magtanong L, Dixon SJ, Watts JL. Dietary Lipids Induce Ferroptosis in Caenorhabditiselegans and Human Cancer Cells. Dev Cell. 2020;54: 447-454.e4. doi:10.1016/J.DEVCEL.2020.06.019

59. Horikawa M, Sakamoto K. Polyunsaturated fatty acids are involved in regulatory mechanism of fatty acid homeostasis via daf-2/insulin signaling in Caenorhabditis elegans. Mol Cell Endocrinol. 2010;323: 183–192. doi:10.1016/J.MCE.2010.03.004

60. Chamoli M, Goyala A, Tabrez SS, Siddiqui AA, Singh A, Antebi A, et al. Polyunsaturated fatty acids and p38-MAPK link metabolic reprogramming to cytoprotective gene expression during dietary restriction. Nature Communications 2020 11:1. 2020;11: 1–13. doi:10.1038/s41467-020-18690-4

61. Liu R, Chen L, Wang Y, Zhang G, Cheng Y, Feng Z, et al. High ratio of ω-3/ω-6 polyunsaturated fatty acids targets mTORC1 to prevent high-fat diet-induced metabolic syndrome and mitochondrial dysfunction in mice. J Nutr Biochem. 2020;79: 108330. doi:10.1016/J.JNUTBIO.2019.108330

62. Worgall TS, Sturley SL, Seo T, Osborne TF, Deckelbaum RJ. Polyunsaturated fatty acids decrease expression of promoters with sterol regulatory elements by decreasing levels of mature sterol regulatory element-binding protein. J Biol Chem. 1998;273: 25537–25540. doi:10.1074/JBC.273.40.25537

63. Yahagi N, Shimano H, Hasty AH, Amemiya-Kudo M, Okazaki H, Tamura Y, et al. A crucial role of sterol regulatory element-binding protein-1 in the regulation of lipogenic gene expression by polyunsaturated fatty acids. J Biol Chem. 1999;274: 35840–35844. doi:10.1074/JBC.274.50.35840

64. Wang Y, Li C, Zhang J, Xu X, Fu L, Xu J, et al. Polyunsaturated fatty acids promote the rapid fusion of lipid droplets in Caenorhabditis elegans. Journal of Biological Chemistry. 2022;298: 102179. doi:10.1016/j.jbc.2022.102179

65. Kahn-Kirby AH, Dantzker JLM, Apicella AJ, Schafer WR, Browse J, Bargmann CI, et al. Specific polyunsaturated fatty acids drive TRPV-dependent sensory signaling in vivo. Cell. 2004;119: 889–900. doi:10.1016/j.cell.2004.11.005

66. Marza E, Lesa GM. Polyunsaturated fatty acids and neurotransmission in Caenorhabditis elegans. Biochem Soc Trans. 2006;34: 77–80. doi:10.1042/BST0340077

67. Vásquez V, Krieg M, Lockhead D, Goodman MB. Phospholipids that contain polyunsaturated fatty acids enhance neuronal cell mechanics and touch sensation. Cell Rep. 2014;6: 70. doi:10.1016/J.CELREP.2013.12.012

68. Chen WW, Yi YH, Chien CH, Hsiung KC, Ma TH, Lin YC, et al. Specific polyunsaturated fatty acids modulate lipid delivery and oocyte development in C. elegans revealed by molecular-selective label-free imaging. Sci Rep. 2016;6. doi:10.1038/SREP32021

69. Wu Y, Zhang Y, Jiao J. The relationship between n-3 polyunsaturated fatty acids and telomere: A review on proposed nutritional treatment against metabolic syndrome and potential signaling pathways. Crit Rev Food Sci Nutr. 2024;64: 4457–4476. doi:10.1080/10408398.2022.2142196

70. Perez CL, Van Gilst MR. A 13C Isotope Labeling Strategy Reveals the Influence of Insulin Signaling on Lipogenesis in C. elegans. Cell Metab. 2008;8: 266–274. doi:10.1016/j.cmet.2008.08.007

71. Plays M, Müller S, Rodriguez R. Chemistry and biology of ferritin. Metallomics. 2021;13: 21. doi:10.1093/MTOMCS/MFAB021

72. Jenkins NL, James SA, Salim A, Sumardy F, Speed TP, Conrad M, et al. Changes in ferrous iron and glutathione promote ferroptosis and frailty in aging caenorhabditis elegans. Elife. 2020;9: 1–28. doi:10.7554/ELIFE.56580

73. Pekec T, Lewandowski J, Komur AA, Sobańska D, Guo Y, Świtońska-Kurkowska K, et al. Ferritin-mediated iron detoxification promotes hypothermia survival in Caenorhabditis elegans and murine neurons. Nature Communications 2022 13:1. 2022;13: 1–19. doi:10.1038/s41467-022-32500-z

74. Shen J, Wu G, Tsai AL, Zhou M. Structure and Mechanism of a Unique Diiron Center in Mammalian Stearoyl-CoA Desaturase. J Mol Biol. 2020;432: 5152–5161. doi:10.1016/J.JMB.2020.05.017

75. Sperling P, Ternes P, Zank TK, Heinz E. The evolution of desaturases. Prostaglandins Leukot Essent Fatty Acids. 2003;68: 73–95. doi:10.1016/S0952-3278(02)00258-2

76. Zhu XG, Nicholson Puthenveedu S, Shen Y, La K, Ozlu C, Wang T, et al. CHP1 Regulates Compartmentalized Glycerolipid Synthesis by Activating GPAT4. Mol Cell. 2019;74: 45-58.e7. doi:10.1016/j.molcel.2019.01.037

77. Lesa GM, Palfreyman M, Hall DH, Clandinin MT, Rudolph C, Jorgensen EM, et al. Long chain polyunsaturated fatty acids are required for efficient neurotransmission in C. elegans. J Cell Sci. 2003;116: 4965–4975. doi:10.1242/JCS.00918

78. Sherratt SCR, Juliano RA, Copland C, Bhatt DL, Libby P, Mason RP. EPA and DHA containing phospholipids have contrasting effects on membrane structure. J Lipid Res. 2021;62: 100106. doi:10.1016/J.JLR.2021.100106

79. Chiang N, Serha CN. Specialized pro-resolving mediator network: an update on production and actions. Essays Biochem. 2020;64: 443–462. doi:10.1042/EBC20200018

80. Tanaka T, Izuwa S, Tanaka K, Yamamoto D, Takimoto T, Matsuura F, et al. Biosynthesis of 1,2-dieicosapentaenoyl-sn-glycero-3-phosphocholine in Caenorhabditis elegans. Eur J Biochem. 1999;263: 189–195. doi:10.1046/J.1432-1327.1999.00480.X

81. Kulas J, Schmidt C, Rothe M, Schunck WH, Menzel R. Cytochrome P450-dependent metabolism of eicosapentaenoic acid in the nematode Caenorhabditis elegans. Arch Biochem Biophys. 2008;472: 65–75. doi:10.1016/J.ABB.2008.02.002

82. Mokoena NZ, Sebolai OM, Albertyn J, Pohl CH. Synthesis and function of fatty acids and oxylipins, with a focus on Caenorhabditis elegans. Prostaglandins Other Lipid Mediat. 2020;148. doi:10.1016/J.PROSTAGLANDINS.2020.106426

83. Kosel M, Wild W, Bell A, Rothe M, Lindschau C, Steinberg CEW, et al. Eicosanoid formation by a cytochrome P450 isoform expressed in the pharynx of Caenorhabditis elegans. Biochemical Journal. 2011;435: 689–700. doi:10.1042/BJ20101942

84. Hoang HD, Prasain JK, Dorand D, Miller MA. A Heterogeneous Mixture of F-Series Prostaglandins Promotes Sperm Guidance in the Caenorhabditis elegans Reproductive Tract. PLoS Genet. 2013;9: e1003271. doi:10.1371/JOURNAL.PGEN.1003271

85. Sulston J, Hodgkin J. The Nematode Caenorhabditis elegans. Wood W, editor. Cold Spring Harbor Laboratory Press; 1988.

86. Depristo MA, Banks E, Poplin R, Garimella K V., Maguire JR, Hartl C, et al. A framework for variation discovery and genotyping using next-generation DNA sequencing data. Nature Genetics 2011 43:5. 2011;43: 491–498. doi:10.1038/ng.806

87. McKenna A, Hanna M, Banks E, Sivachenko A, Cibulskis K, Kernytsky A, et al. The Genome Analysis Toolkit: A MapReduce framework for analyzing next-generation DNA sequencing data. Genome Res. 2010;20: 1297–1303. doi:10.1101/GR.107524.110

88. Cingolani P, Platts A, Wang LL, Coon M, Nguyen T, Wang L, et al. A program for annotating and predicting the effects of single nucleotide polymorphisms, SnpEff: SNPs in the genome of Drosophila melanogaster strain w1118; iso-2; iso-3. Fly (Austin). 2012;6: 80–92. doi:10.4161/FLY.19695

89. Ghanta KS, Mello CC. Melting dsDNA Donor Molecules Greatly Improves Precision Genome Editing in Caenorhabditis elegans. Genetics. 2020;216: 643–650. doi:10.1534/GENETICS.120.303564

90. Dokshin GA, Ghanta KS, Piscopo KM, Mello CC. Robust Genome Editing with Short Single-Stranded and Long, Partially Single-Stranded DNA Donors in Caenorhabditis elegans. Genetics. 2018;210: 781–787. doi:10.1534/GENETICS.118.301532

91. Devkota R, Pilon M. FRAP: A Powerful Method to Evaluate Membrane Fluidity in Caenorhabditis elegans. Bio Protoc. 2018;8. doi:10.21769/BIOPROTOC.2913

92. Löfgren L, Forsberg GB, Ståhlman M. The BUME method: a new rapid and simple chloroform-free method for total lipid extraction of animal tissue. Scientific Reports 2016 6:1. 2016;6: 1–11. doi:10.1038/srep27688

93. Jung HR, Sylvänne T, Koistinen KM, Tarasov K, Kauhanen D, Ekroos K. High throughput quantitative molecular lipidomics. Biochim Biophys Acta. 2011;1811: 925–934. doi:10.1016/J.BBALIP.2011.06.025

94. Ekroos K, Ejsing CS, Bahr U, Karas M, Simons K, Shevchenko A. Charting molecular composition of phosphatidylcholines by fatty acid scanning and ion trap MS3 fragmentation. J Lipid Res. 2003;44: 2181–2192. doi:10.1194/JLR.D300020-JLR200

95. Ejsing CS, Sampaio JL, Surendranath V, Duchoslav E, Ekroos K, Klemm RW, et al. Global analysis of the yeast lipidome by quantitative shotgun mass spectrometry. Proc Natl Acad Sci U S A. 2009;106: 2136–2141. doi:10.1073/PNAS.0811700106

FIGURES AND SUPPLEMENTARY FIGURES

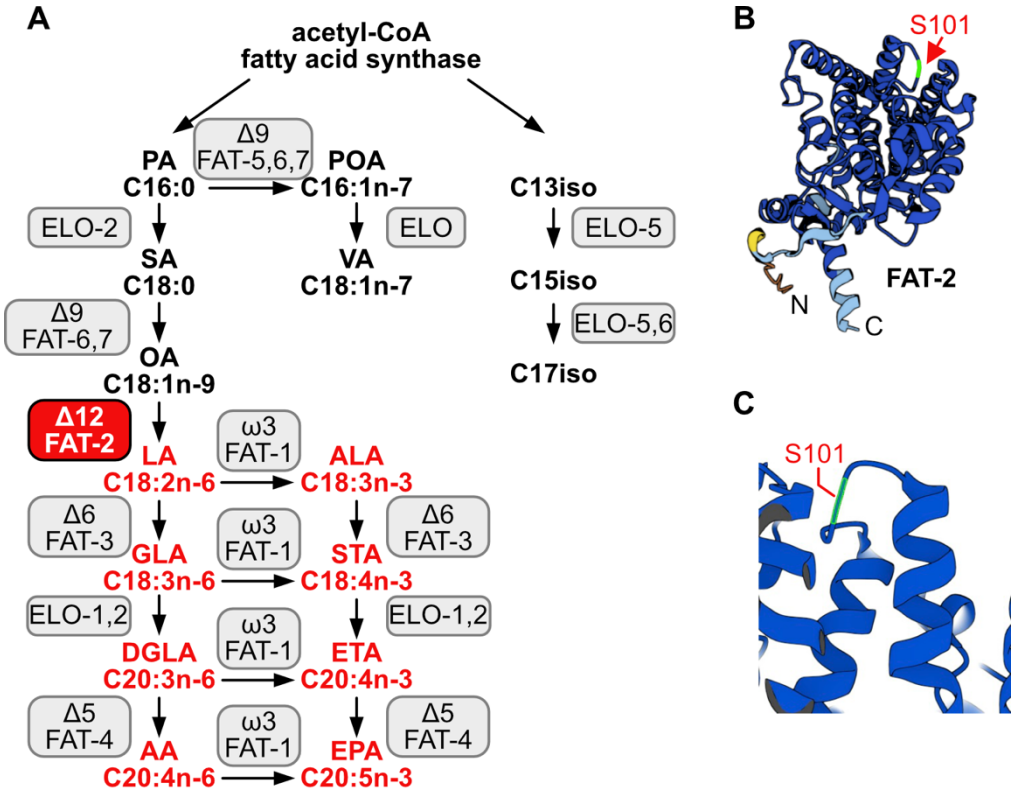

Fig 1. *C. elegans* fatty acid synthesis pathway and FAT-2 desaturase. (A) Simplified pathway of fatty acid synthesis and desaturation in *C. elegans.* Boxes indicate the name of the enzymes, FAT-2 desaturase is indicated in a red box. Fatty acids of which the synthesis is dependent on FAT-2 are indicated in red. Fatty acid abbreviations are as follow: palmitic acid (PA), palmitoleic acid (POA), vaccenic acid (VA), stearic acid (SA), oleic acid (OA), linoleic acid (LA), alpha-linolenic acid (ALA), gamma-linolenic acid (GLA), stearidonic acid (STA), dihomo-gamma-linolenic acid (DGLA), eicosatetraenoic acid (ETA), arachidonic acid (AA), and eicosapentaenoic acid (EPA). **(B)** AlphaFold2 predicted FAT-2 structure with the serine at position 101 indicated with a red arrow. **(C)** Same structure as in B, zoomed in and angled to show that the S101 position that is mutated to phenylalanine in the *fat-2(wa17)* allele lies in a loop connecting two alpha helices.

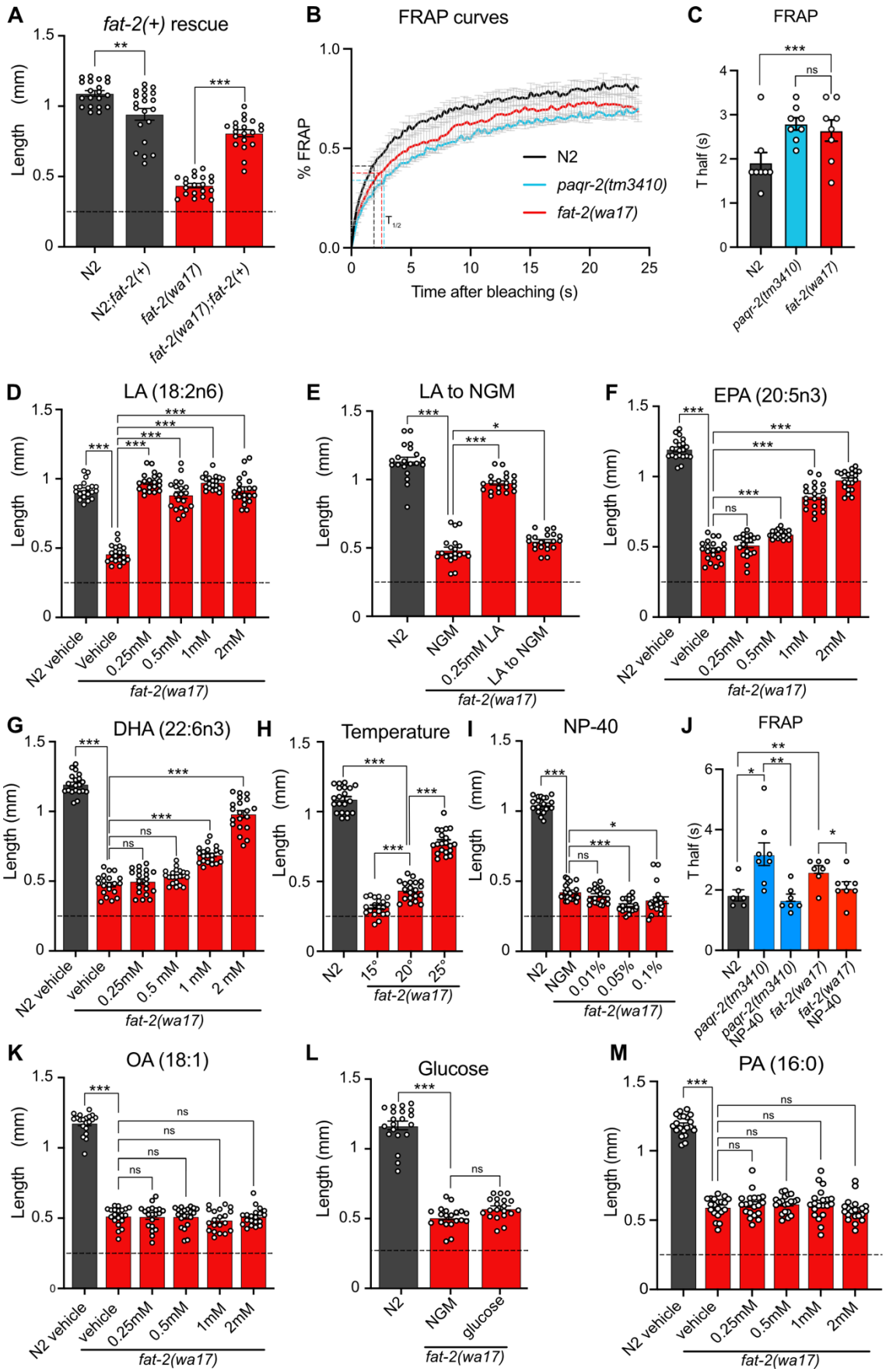

Fig 2. Characterization and rescue of *fat-2(wa17)*. (A) Introduction of the wild-type *fat-2(+)* allele on an extrachromosomal array rescues the *fat-2(wa17)* growth defect. **(B-C)** FRAP curve and T_{half} value

show that *fat-2(wa17)* has rigid membranes similar to *paqr-2(tm3410)* control. **(D-I,K-M)** The lengths of *fat-2(wa17)* worms grown from L1 stage for 72h in the indicated conditions; horizontal dashed lines indicate the approximate lengths of the synchronized L1s at the start of the experiments. n=20 for each genotype/condition. **(J)** FRAP T_{half} values show that NP-40 rescues *fat-2(wa17)* rigid membranes similar to *paqr-2(tm3410).* Error bars show the standard error of the mean. *$p < 0.05$, **$p < 0.01$, ***$p < 0.001$ indicate significant differences compared to the *fat-2(wa17)* control.

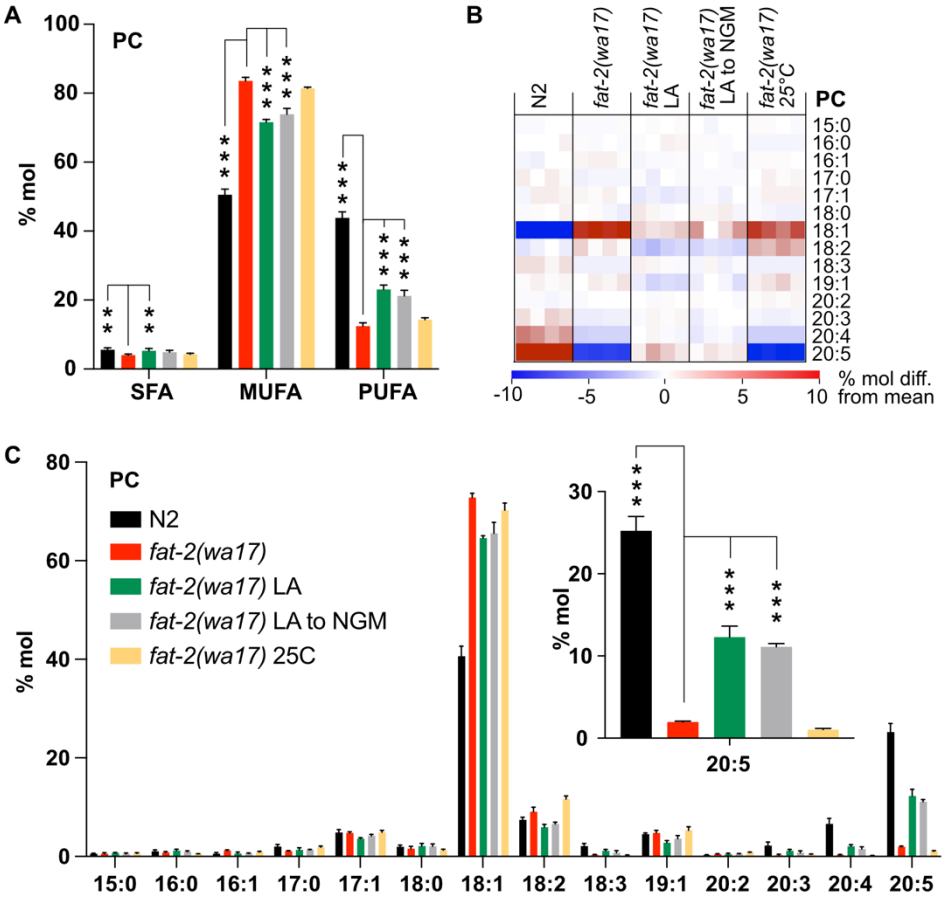

Fig 3. Lipidomic analysis of *fat-2(wa17)* mutant. (A) SFA, MUFA, and PUFA levels in phosphatidylcholines (PCs) of *fat-2(wa17)* grown in various conditions. Note that cultivation on 2mM LA boosts PUFA levels. LA to NGM worms were grown on 2 mM LA before being transferred to NGM 6 h prior to harvesting. **(B)** Heatmap of PC species in *fat-2(wa17)* in all conditions. **(C)** Levels of individual FA species in PCs for all conditions. Inset shows levels of 20:5 FA are increased by providing *fat-2(wa17)* with linoleic acid. *p < 0.05, **p < 0.01, ***p < 0.001 indicate significant differences compared to the *fat-2(wa17)* control.

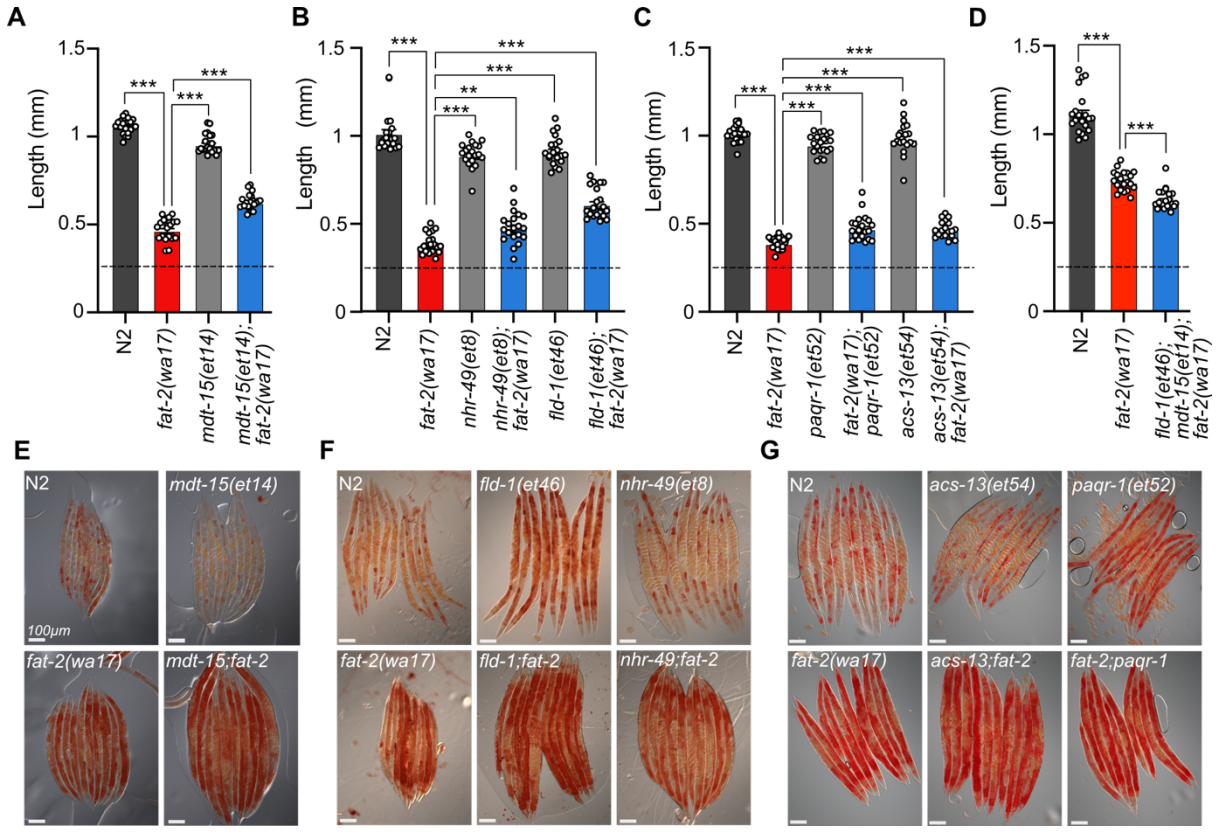

Fig 4. Membrane fluidizing mutations partially rescue *fat-2(wa17)*. (A-D) Fluidizing *paqr-2(tm3410)* suppressor mutations only slightly rescue *fat-2(wa17)* growth. Dashed horizontal lines indicate approximate length of L1s at the start of the experiments; length was measured 72 h post-synchronization. Error bars show the standard error of the mean. *p < 0.05, **p < 0.01, ***p < 0.001 indicate significant differences compared to the *fat-2(wa17)* control. **(E-G)** Oil Red O staining of day 1 adults shows that the high lipid abundance in *fat-2(wa17)* is not suppressed by *paqr-2(tm3410)* fluidizing mutations.

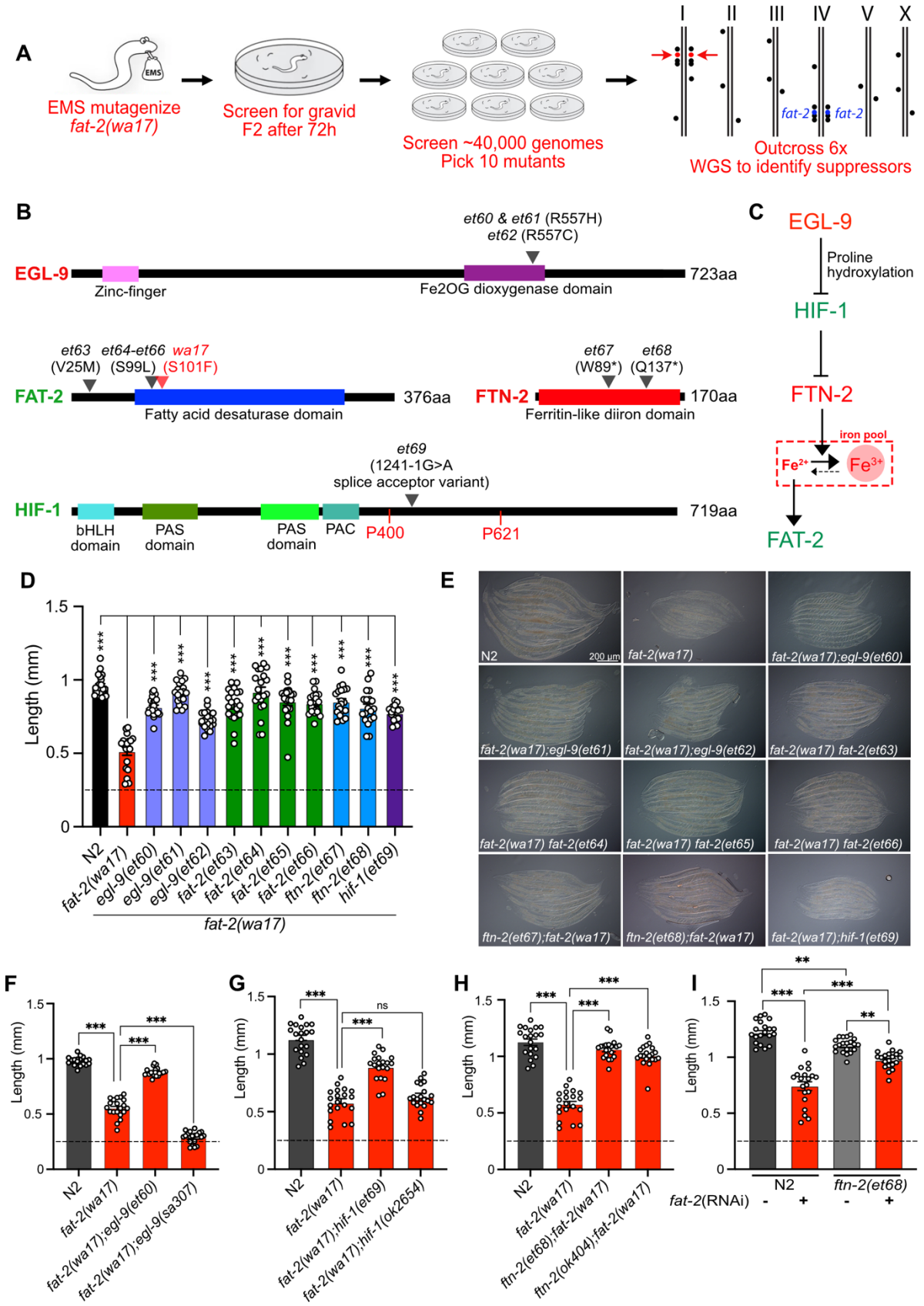

Fig 5. A forward genetic screen reveals *fat-2(wa17)* is suppressed by mutations in the HIF-1 pathway. (A) Overview of the forward genetics screen strategy to isolate *fat-2(wa17)* suppressors. **(B)**

Identity and position of the *fat-2(wa17)* suppressors as well as the positions of functional domains. Novel mutations are marked by a black triangle with corresponding allele name and mutation effect; the red triangle in FAT-2 indicates the original *wa17* allele. Gene names in red represent loss- or reduction-of-function mutations; gene names in green represent gain-of-function mutations. **(C)** Proposed pathway of *fat-2(wa17)* suppression by mutations in the HIF-1 pathway. Reduction of EGL-9 constitutively activates HIF-1, HIF-1 activation inhibits FTN-2. The loss of FTN-2 increases the levels of Fe^{2+} outside of iron pools, thus boosting FAT-2 desaturase activity. Gain-of-function mutations are labeled in green, loss- or reduction-of-function mutations are labeled in red. **(D)** Length of all *fat-2(wa17)* suppressors measured 72 h after L1 stage. **(E)** Representative images of *fat-2(wa17)* suppressors after 72 h of growth. **(F-H)** Null alleles of *egl-9* and *hif-1* do not rescue *fat-2(wa17)*, but the null allele of *ftn-2* does, confirming that *ftn-2(et67)* and *ftn-2(et68*) are loss-of-function alleles. Lengths measured 72 h after L1 synchronization. **(I)** *ftn-2(et68)* rescue of *fat-2(RNAi)* worms confirming that the suppressors are not *wa17* specific. The horizontal dashed line indicates the approximate length of L1s at the start of each experiment. Error bars show the standard error of the mean. $*p < 0.05$, $**p < 0.01$, $***p < 0.001$ indicate significant differences compared to the *fat-2(wa17)* control.

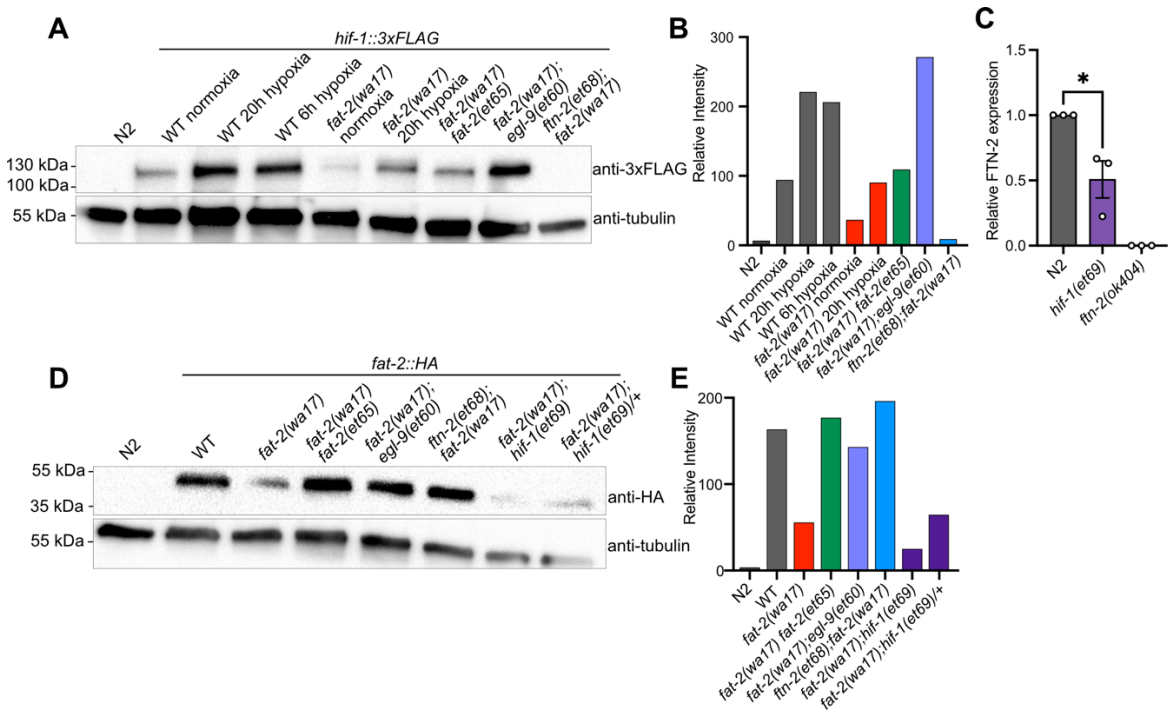

Fig 6. *fat-2(wa17)* suppressors belong in HIF-1 pathway and influence HIF-1 levels. (A) Western blot confirming that *hif-1::3xFLAG* levels in *fat-2(wa17*) is increased by *egl-9(et60),* but not by *ftn-2(et68)*. Hypoxia treatment increases HIF-1 levels in WT and *fat-2(wa17)*, confirming successful protein tagging. **(B)** Quantification of Western blot in **A** showing normalized relative intensity of the HIF-1 signal to that of tubulin. **(C)** mRNA expression of FTN-2 confirming that hif-1(et69) reduces FTN-2 levels. **(D)** Western blot confirming that *fat-2::HA* levels *in fat-2(wa17)* are greatly reduced but increased in suppressor strains. **(E)** Quantification of Western blot in D showing normalized relative intensity of the FAT-2 signal to that of tubulin.

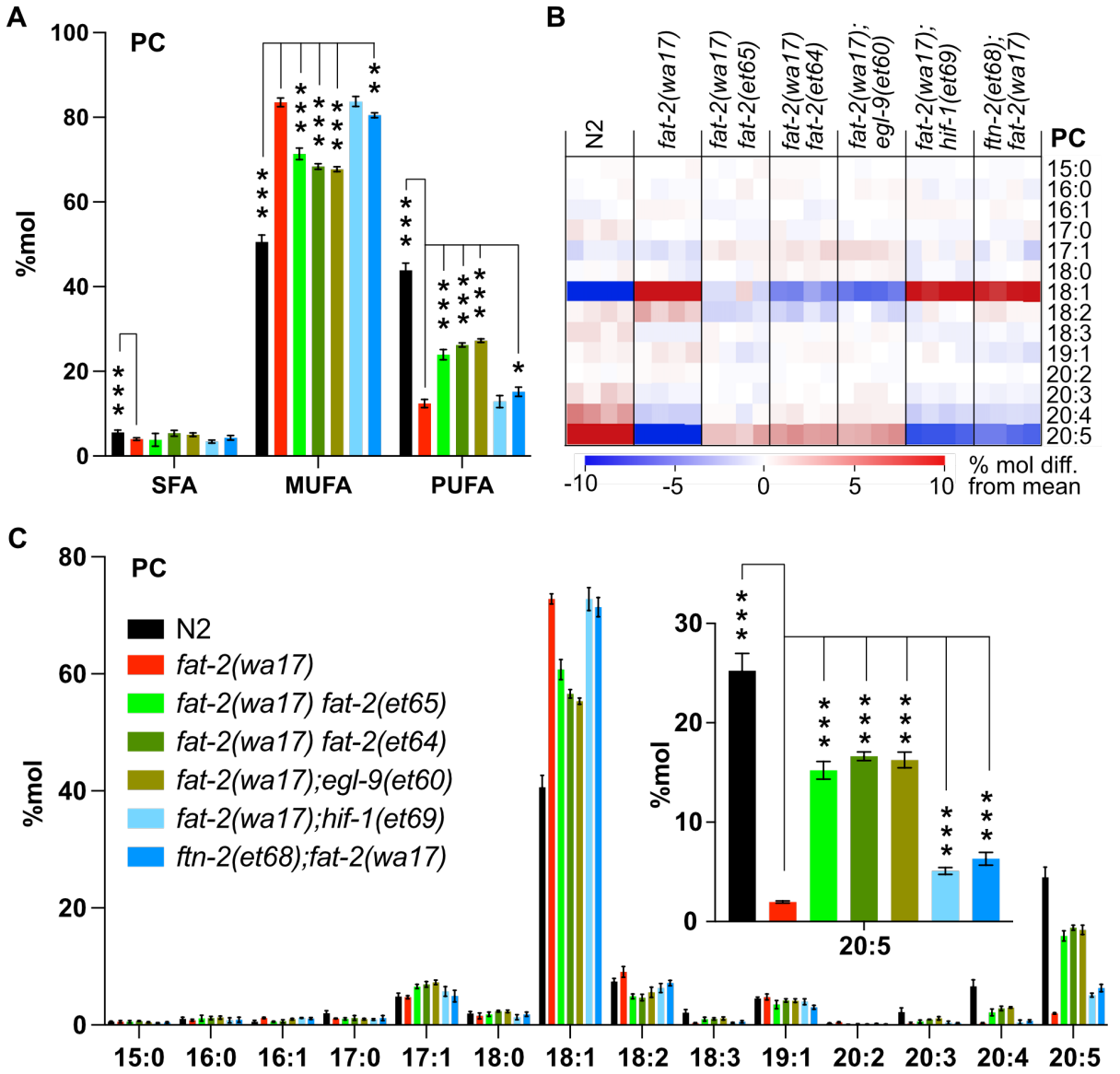

Fig 7. Lipidomic analysis of *fat-2(wa17)* suppressors reveals that PUFA levels are increased. (A) Levels of SFAs, MUFAs, and PUFAs in PCs measured in *fat-2(wa17)* suppressors confirming that the suppressors increase PUFA levels in *fat-2(wa17)*. Worms were homozygous for all indicated genotypes but note that the *hif-1(et69)* allele suppresses *fat-2(wa17)* best in a heterozygous state. **(B)** Heat map analysis of PC species in suppressor mutants. **(C)** Levels of individual FA species in PCs in *fat-2(wa17)* suppressors, insert shows that levels of C20:5 are significantly increased in all double mutant strains. *$p < 0.05$, **$p < 0.01$, ***$p < 0.001$ indicate significant differences compared to the *fat-2(wa17)* control. Note that the N2 and *fat-2(wa17)* samples are the same as in Fig 3.

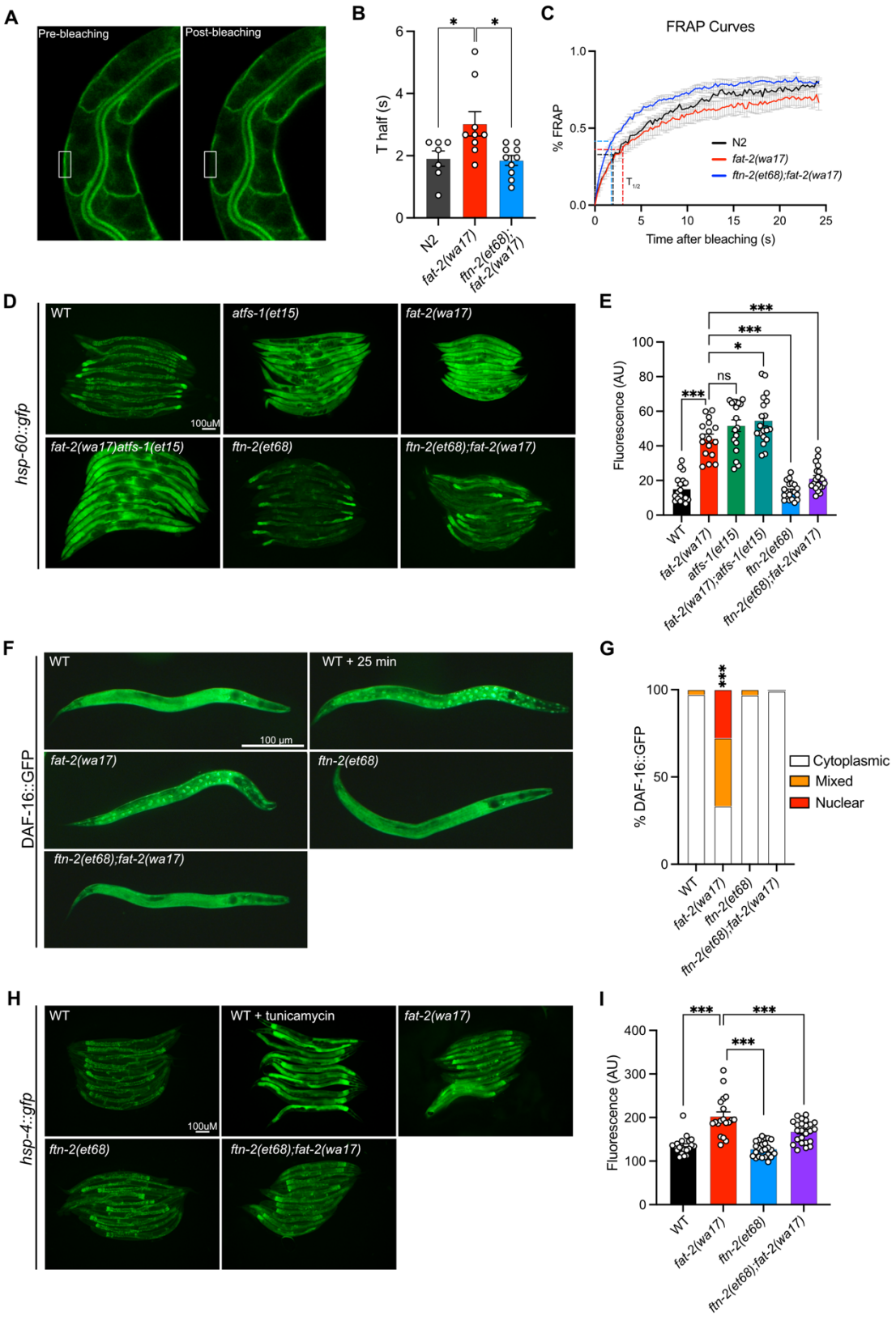

Fig 8. *ftn-2(et68)* rescues *fat-2(wa17)*'s stress responses. **(A)** Representative image of a FRAP experiment, showing pGLO-1::GFP-CAAX-positive intestinal membranes. The rectangle indicates the bleached area. **(B-C)** T_{half} values and FRAP curves showing that *ftn-2(et68);fat-2(wa17)* has less rigid membranes than *fat-2(wa17)*. **(D-E)** Representative images and quantification of *ftn-2(et68)* rescue of

fat-2(wa17) mitochondrial stress with a *hsp-60::gfp* reporter. *atfs-1(et15)* serves as a control for high mitochondrial UPR activation. **(F-G**) Representative images and quantification of DAF-16::GFP localization showing that the DAF-16 stress response is constitutively active in the *fat-2(wa17)* mutant but normalized by *ftn-2(et68*). Chi-squared test shows that *fat-2(wa17)* is significantly different from WT. **(H-I)** Representative images and quantification of mild ER stress in *fat-2(wa17)* that is slightly rescued by *ftn-2(et68*) using a *hsp-4::gfp* reporter. *$p < 0.05$, **$p < 0.01$, ***$p < 0.001$ indicate significant differences compared to the *fat-2(wa17)* control.

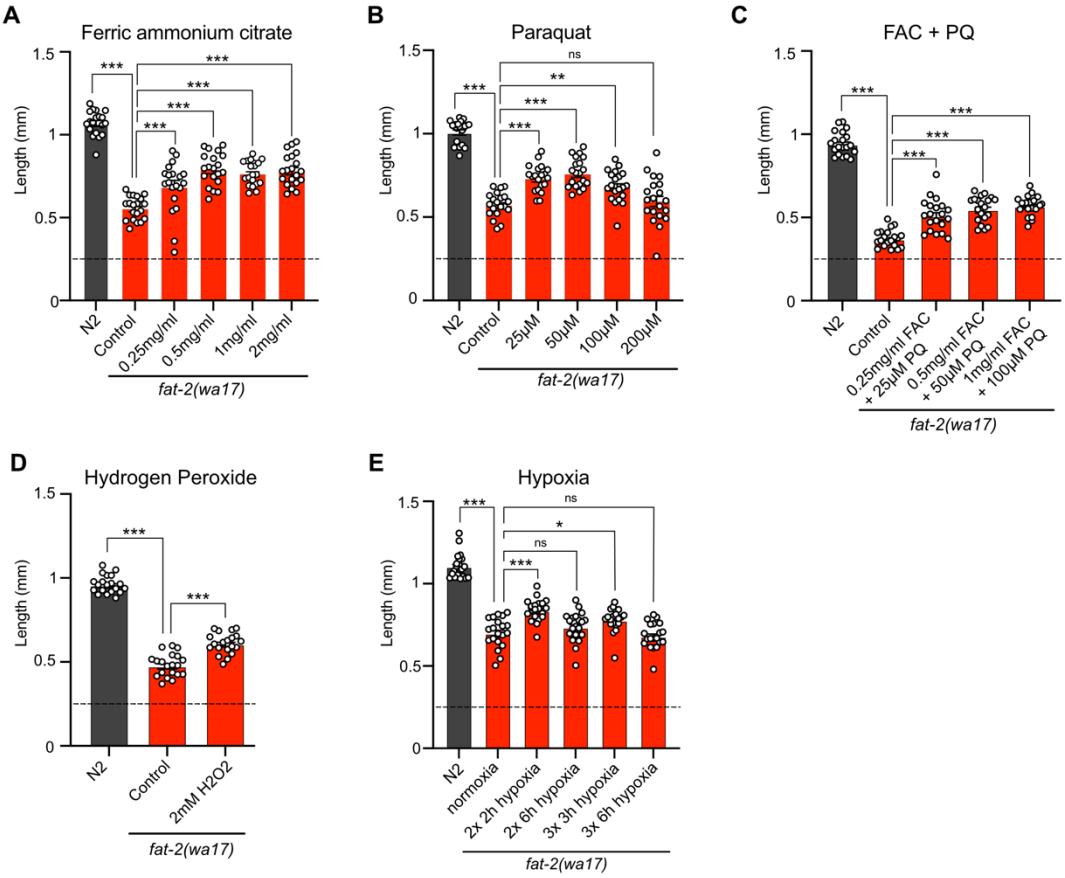

Fig 9. Exogenous treatments that mimic *fat-2(wa17)* suppressors partially rescue *fat-2(wa17)*. (A-E) Length assay of *fat-2(wa17)* cultivated with different treatments for 72 h after L1 stage synchronization. The horizontal dashed line represents the approximate length of L1 worms at start of each experiment. *p < 0.05, **p < 0.01, ***p < 0.001 indicate significant differences compared to the *fat-2(wa17)* control.

SUPPLEMENTARY FIGURES

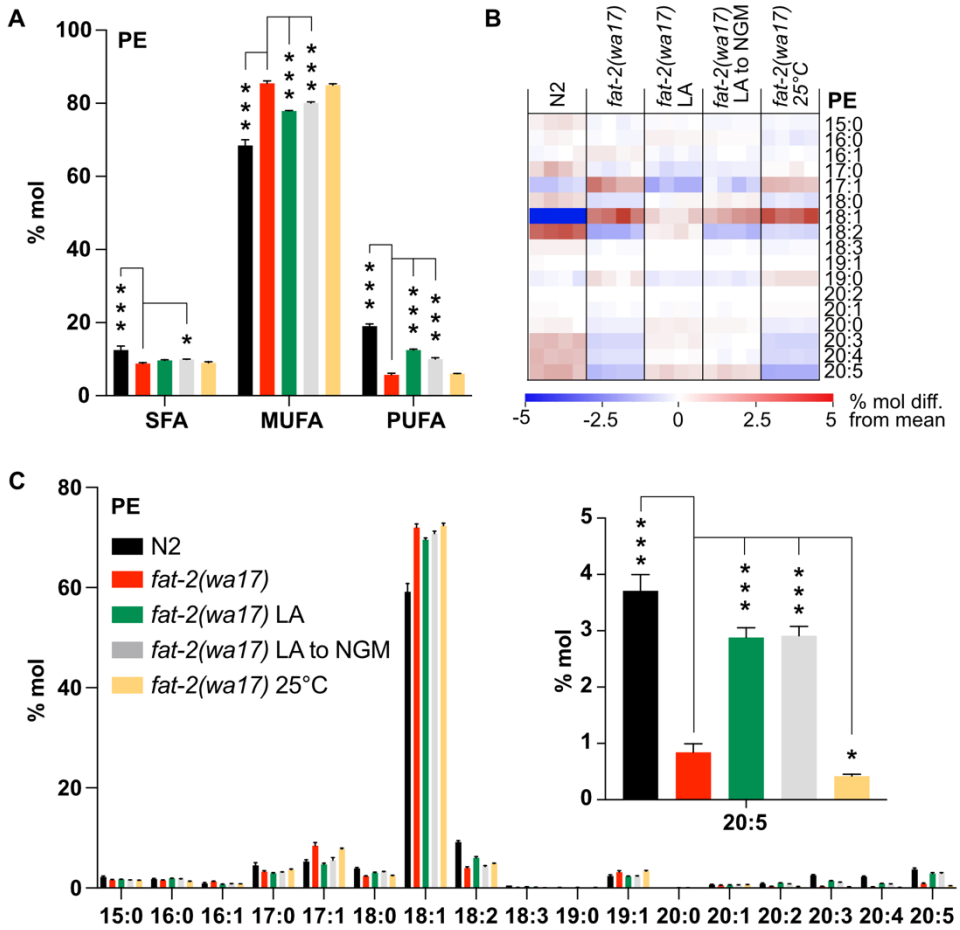

S1 Fig. Lipidomics analysis of PEs in *fat-2(wa17)* in various cultivation conditions. (A) SFA, MUFA, and PUFA levels in phosphatidylethanolamine (PEs) of *fat-2(wa17)* grown in various conditions. Cultivation on 2 mM LA boosts PUFA levels. LA to NGM worms were grown on 2 mM LA before being transferred to NGM 6 h prior to harvesting. **(B)** Heatmap of PE species in *fat-2(wa17)* in all conditions. **(C)** Levels of individual FA species in PEs for all conditions. Inset shows that the levels of C20:5 are increased by providing *fat-2(wa17)* with LA. *$p < 0.05$, **$p < 0.01$, ***$p < 0.001$ indicate significant differences compared to the *fat-2(wa17)* control.

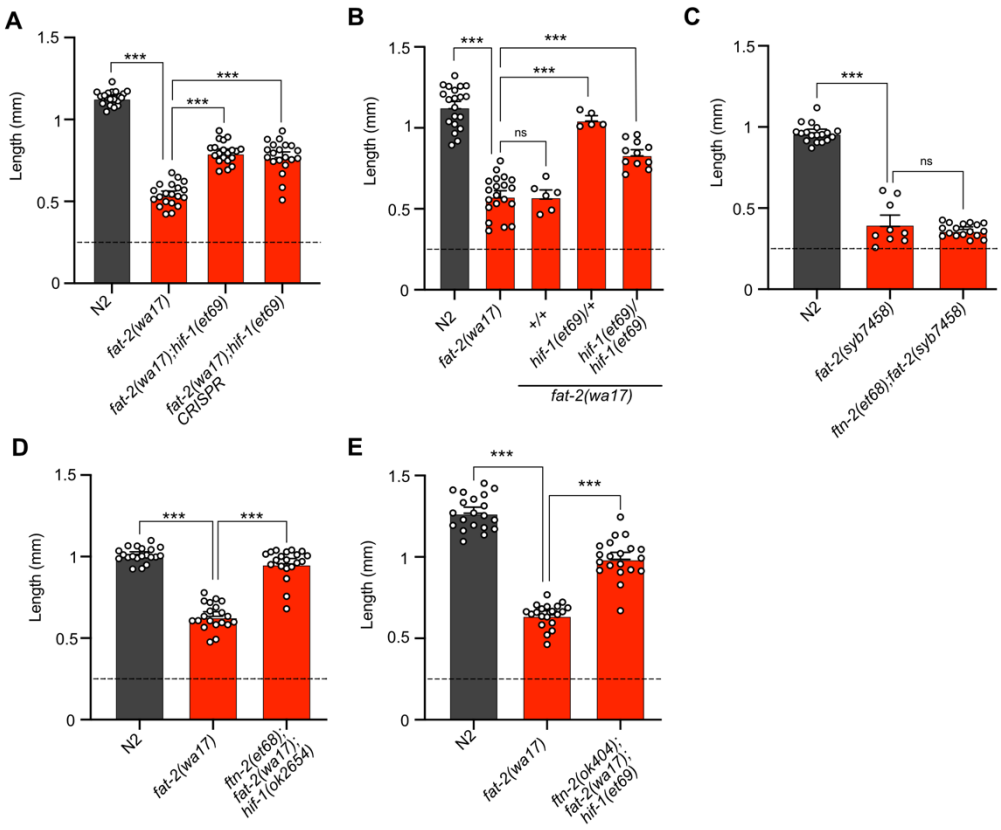

S2 Fig. *fat-2(wa17)* and *fat-2(syb7458)* with suppressors. (A) Confirmation of *hif-1(et69)* suppression of *fat-2(wa17)* by CRISPR-Cas9. **(B)** The *hif-1(et69)* allele acts best as a *fat-2(wa17)* suppressor when in a heterozygous state. **(C)** *ftn-2(et68)* does not act as a suppressor for the *fat-2(syb7458)* allele. **(D)** *ftn-2(et68)* still suppresses *fat-2(wa17)* in a *hif-1* null background. **(E)** *hif-1(et69)* suppresses *fat-2(wa17)* in a *ftn-2* null background. **(A-E)** All length measurements were taken 72 h after L1 synchronization. Horizontal dashed line represents the approximate size of L1s at the start of each experiment. Error bars show the standard error of the mean. *$p < 0.05$, **$p < 0.01$, ***$p < 0.001$ indicate significant differences compared to the *fat-2(wa17)* control.

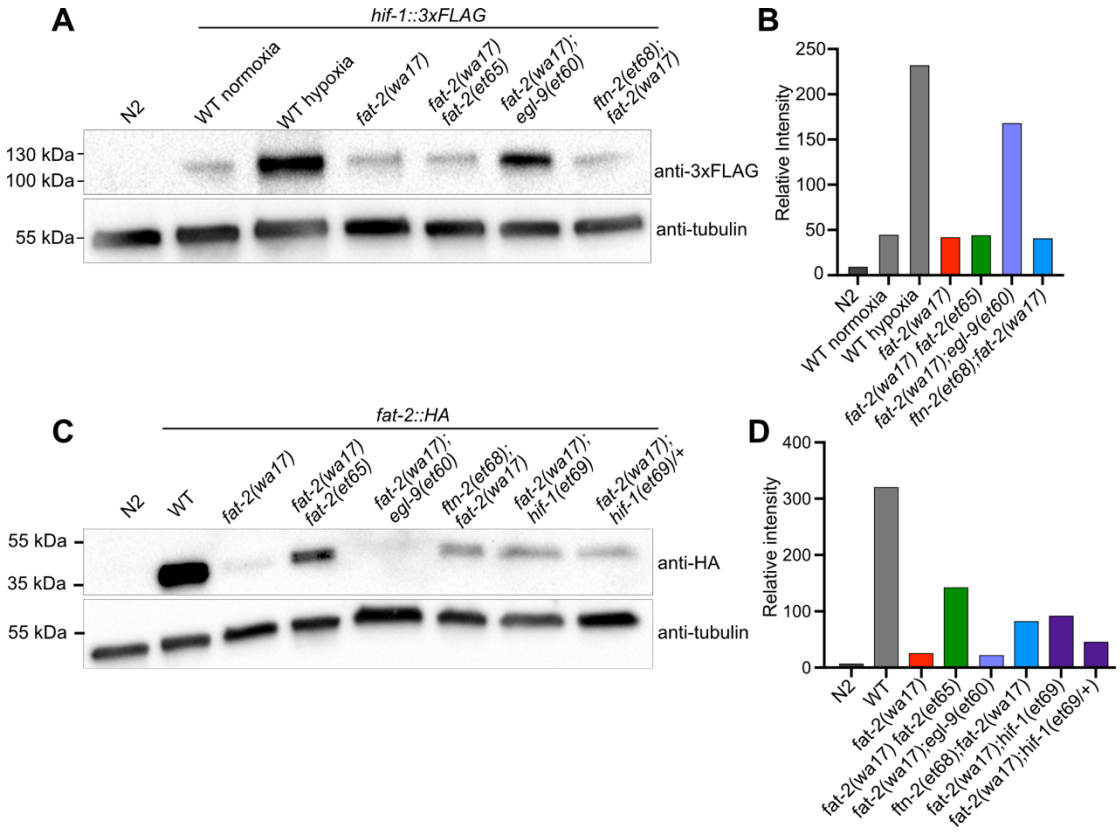

S3 Fig. Suppressors influence HIF-1 and FAT-2 levels. (A) Western blot showing that *hif-1::3xFLAG* levels in *fat-2(wa17)* are increased by *egl-9(et60)*. **(B)** Quantification of Western blot in A showing normalized relative intensity of the HIF-1 signal to that of tubulin. **(C)** Western blot showing that *fat-2::HA* levels are reduced in *fat-2(wa17)* but increased by suppressors. **(D)** Quantification of Western blot in C showing normalized relative intensity of HIF-1 signal to that of tubulin.

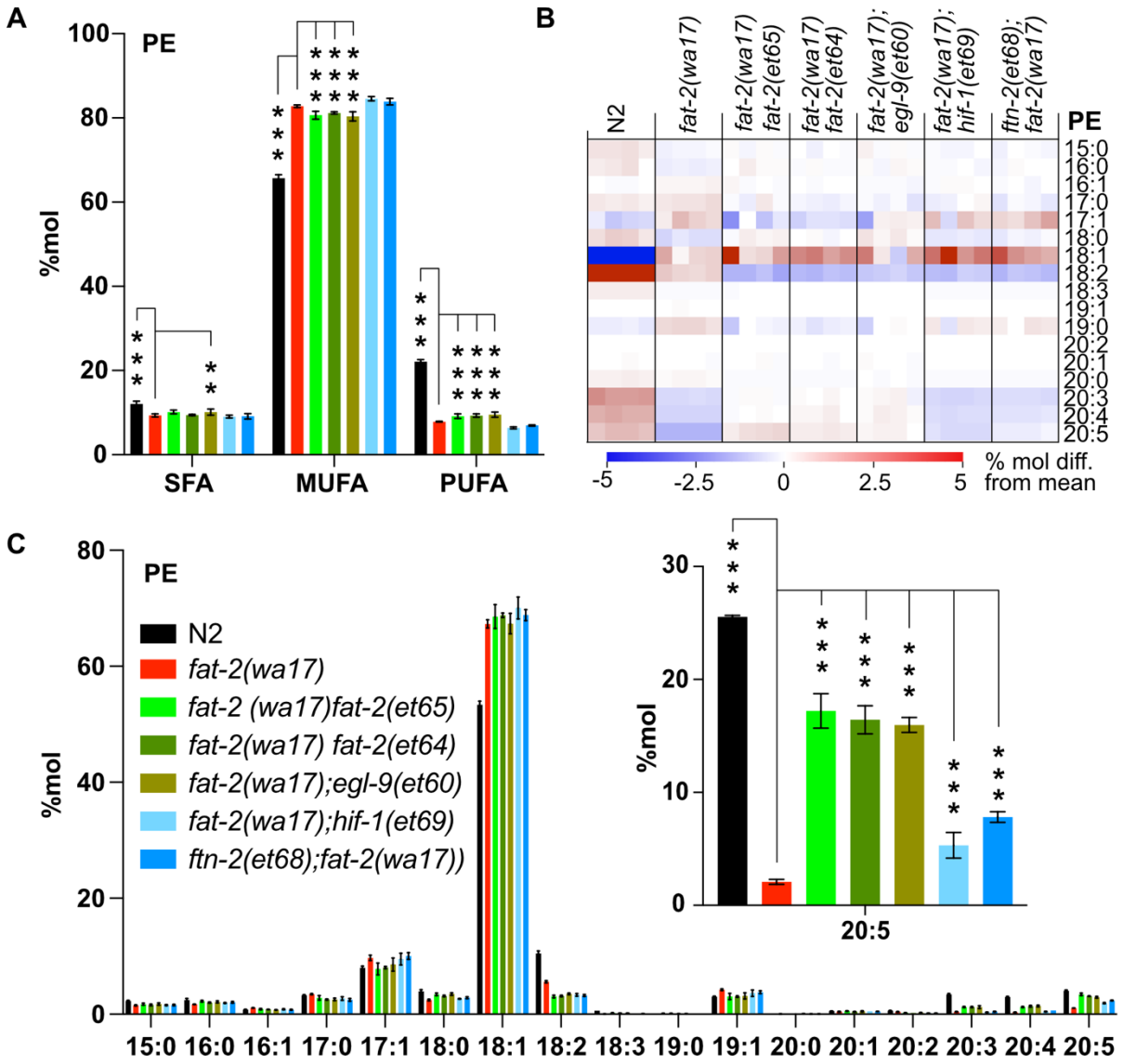

S4 Fig. Lipidomics of PEs in *fat-2(wa17)* suppressors. (A) Levels of SFAs, MUFAs, and PUFAs in PEs measured in *fat-2(wa17)* suppressors confirming that the suppressors increase PUFA levels in *fat-2(wa17)*. **(B)** Heat map analysis of PE species in suppressor mutants. **(C)** Levels of individual FA species in PEs in *fat-2(wa17)* suppressors, insert shows levels of 20:5 are increased in all double mutant strains. *$p < 0.05$, **$p < 0.01$, ***$p < 0.001$ indicate significant differences compared to the *fat-2(wa17)* control.

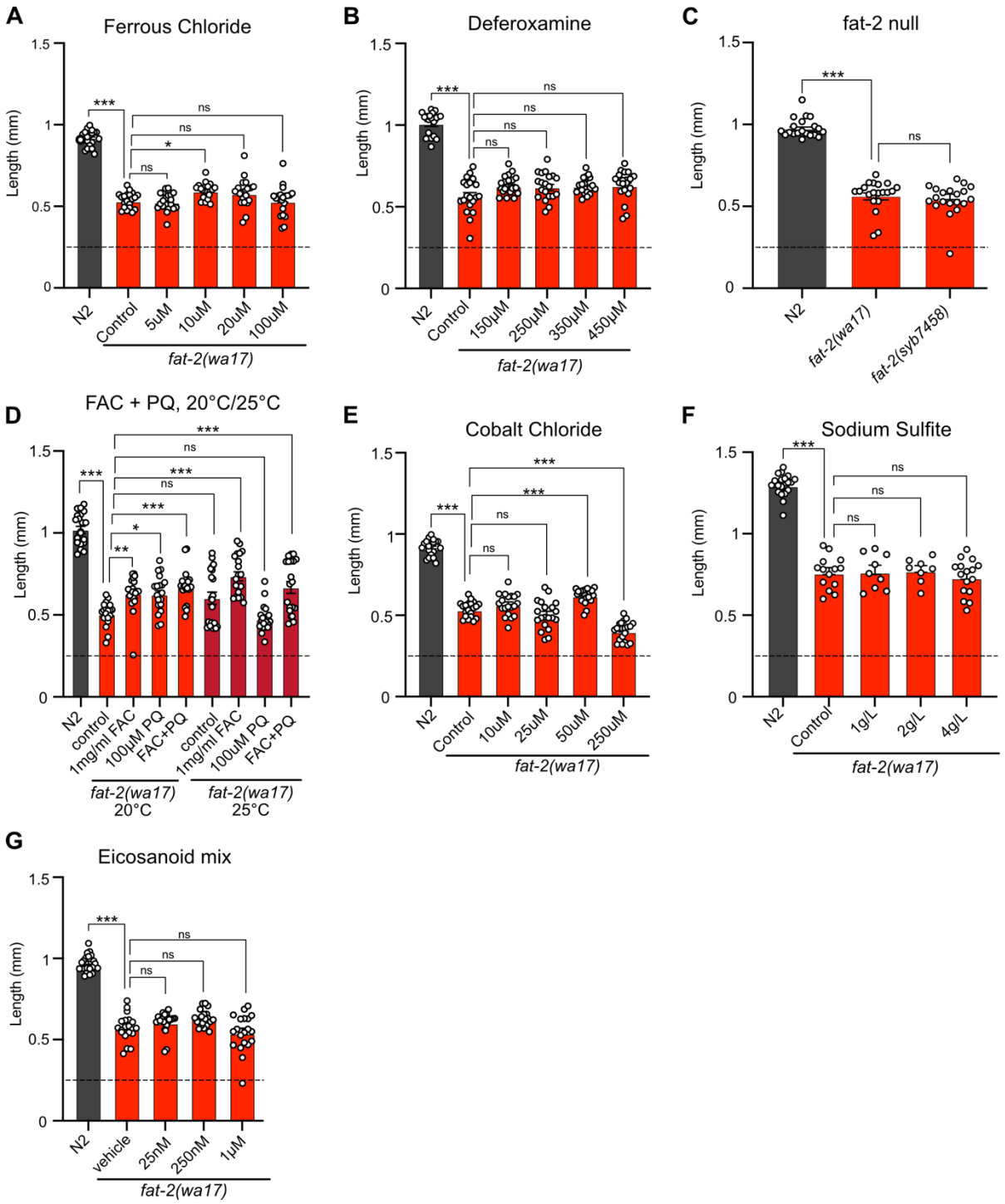

S5 Fig. Exogenous treatment of *fat-2(wa17)* to mimic suppressors. (A-E) Length of *fat-2(wa17)* treated with various diets for 72 h after L1 synchronization attempting to mimic effects of *egl-9*, *ftn-2*, and *hif-1* suppressors. Horizontal dashed line represents approximate size of worms at the start of each experiment. *p < 0.05, **p < 0.01, ***p < 0.001 indicate significant differences compared to the *fat-2(wa17)* control.

S1 Table. *fat-2(wa17)* suppressor genotyping primers.

Allele	Primer	Sequence	Expected product (bp)	Annealing temperature
fat-2(wa17)	Fwd	5' GACAATCGCTACAAAAGTG 3'	320	55°C
	WT Rev	5' CATTGAGCCATTCATAATTGG 3'		
	Mut Rev	5' CATTGAGCCATTCATAATTGA 3'		
fat-2(et63)	WT Fwd	5' AGGTACCGGAGCTTCCATTAG 3'	558	55°C
	Mut Fwd	5' AGGTACCGGAGCTTCCATTAA 3'		
	Rev	5' TGACACGATCCTCAGTAGTCTC 3'		
fat-2(et64-et66)	WT Fwd	5' CATGACTGTGGACATGGGTC 3'	334	55°C
	Mut Fwd	5' CATGACTGTGGACATGGGTT 3'		
	Rev	5' TGACACGATCCTCAGTAGTCTC 3'		
egl-9 (et60-et61)	WT Fwd	5' TGCCAGTCTTCCGTCGTCG 3'	739	55°C
	Mut Fwd	5' ATGCCAGTCTTCCGTCGTCA 3'		
	Rev	5' CGAACGACAAAACCGCGAAC 3'		
egl-9(et62)	WT Fwd	5' CATGCCAGTCTTCCGTCGTC 3'	741	57°C
	Mut Fwd	5' CATGCCAGTCTTCCGTCGTT 3'		
	Rev	5' CGAACGACAAAACCGCGAAC 3'		
ftn-2(et67)	WT Fwd	5' AGCCAGAGAATGATGAGCGG 3'	763	55°C
	Mut Fwd	5' AGCCAGAGAATGATGAGCGA 3'		
	Rev	5' AAGCCTTCAAGGCGGTTCCC 3'		
ftn-2(et68)	Fwd	5' ATGTCTCTCGCTCGTCAAAACT 3'	476	55°C
	WT Rev	5' AATAGAATAATCCTCACCTG 3'		
	Mut Rev	5' AATAGAATAATCCTCACCTA 3'		
hif-1(et69)	WT Fwd	5' GTGATTTCTTAACGTGTGTATTTTAG 3'	588	60°C
	Mut Fwd	5' GTGATTTCTTAACGTGTGTATTTTAA 3'		
	Rev	5' CATCATTGCTTCCGATGACTG 3'		